Technical University of Denmark

DTU

Accelerated rain erosion of wind turbine blade coatings

Zhang, Shizhong; Kiil, Søren; Dam-Johansen, Kim; Bernad Jr., Pablo L.

Link back to DTU Orbit

DTU Library
Technical Information Center of Denmark

Accelerated rain erosion of wind turbine blade coatings

Shizhong Zhang
Ph.D. Thesis
August 2014

Accelerated rain erosion of wind turbine blade coatings

Ph.D. Thesis
by
Shizhong Zhang

Supervisors:
Assoc. Prof. Søren Kiil, DTU Chemical Engineering
Prof. Kim Dam-Johansen, DTU Chemical Engineering
Protective R&D Manager, Pablo L Bernad Jr., Hempel A/S

DTU Chemical Engineering
Department of Chemical and Biochemical Engineering

Preface

This dissertation summarizes the outcome of my last 3 years of research and is submitted as a partial fulfillment of the requirements for obtaining the Ph.D. degree at the Technical University of Denmark. The work was carried out at the Combustion and Harmful Emission Control (CHEC) center of the Department of Chemical and Biochemical Engineering at the Technical University of Denmark in collaboration with coating producer Hempel A/S. The work has been supervised by Associate Professor Søren Kiil and Professor Kim Dam-Johansen from CHEC. The external supervision of the work was carried out by Pablo L Bernad Jr. from Hempel A/S. The project was funded by the Technical University of Denmark and the Hempel Foundation.

I would like to thank my main supervisor Søren Kiil for the numerous constructive discussions on the experiments. Søren also spent a lot of time on reviewing and correcting my article manuscripts and literature survey. Without his encouragement and support, the project would not have been conducted at a good pace. I am also grateful to Kim for his valuable suggestions on the project.

I am grateful to Pablo L Bernad Jr. for his correcting on my written English and help to arrange the experiments. I would like to thank Per Aggerholm Sørensen and Sten Nørkjær who used to work for Hempel A/S and took the role as co-supervisor. They always gave fast feedback no matter what I asked for. I would also like to thank all the colleagues whom I worked with in Hempel A/S, all of them were friendly and willing to help. Thank you, Linda, Erik, Jeanne, and Alicia.

I would like to thank colleagues from our workshop and CHEC technicians for the work done during the construction of the rig and the trouble shooting during the operation. Thank you, Ivan, Jens, Michael, Nikolaj and Rasmus.

Thank you also to all the PhD students who gave me advice, shared knowledge and encouraged me during the research.

Finally, I would like to thank my family for their caring and understanding over the last 3 years.

Shizhong Zhang
Kgs. Lyngby, August 2014

Summary

During operation, the fast-moving blades of wind turbines are exposed to continuous impacts with rain droplets, hail, insects, or solid particles. This can lead to erosion of the blades, whereby the electrical efficiency is compromised and expensive repairs may be required. One possible solution to this problem is elastic blade coatings, which are able to absorb the impact energy without crack formation. The purpose of the work presented in this thesis has been to design and construct a laboratory experimentation device, which allows an accelerated and reliable evaluation of existing or novel blade coating formulations. Results of experiments are compared to data obtained in the larger-size whirling arm rig, which is the present industrial standard for blade coating evaluation. The whirling arm rig consists of three fast-moving horizontal rotors rotating in a heavy artificial rain fall.

There are four chapters in the thesis. In chapter 1, a literature survey provides background information to the field. Topics discussed are the global wind energy development, possible wind turbine constructions, blade structures and materials, blade coatings, and liquid erosion mechanisms. In chapter 2, the design, construction and evaluation of a new laboratory setup for fast screening of 22 coating samples simultaneously is described. The device is based on a principle of discrete water jet slugs. A review of previous rain erosion testing equipment is also included. To provide a basis for comparison of the new setup with the whirling arm rig, a dimensional analysis was conducted and experiments with two polyurethane-based blade coatings carried out. Results showed that water jet slug velocity and impact frequency are the most influential parameters on the coating erosion rate. Furthermore, very small coating surface defects, often present on the specimens tested, appeared to play an important role in the erosion mechanism. The evaluation of the coatings under conditions where impact frequency and water hammer pressure were "matched" could not be directly correlated with the results obtained with the whirling arm rig. This may be attributed, among other contributing factors, to the different contact modes in the two setups, i.e. the movement of coated panels against rain drops versus the movement of water drops against coated specimens. The results endorse the complex nature of the rain erosion phenomenon, which is the consequence of the simultaneous combination of complex mechanisms and as such, it is difficult to reproduce at the laboratory scale.

In chapter 3, the experimental investigation was expanded to a study on the effects of three important process parameters on coating erosion: water cushioning, substrate curvature, and water nozzle-coating distance. In addition, to map the influence of physical properties on rain erosion, mechanical measurements to characterize selected blade coatings, including tensile strength, flexibility, impact, hardness, and abrasion experiments, were conducted. The investigations showed that in some cases water cushioning (the presence of a liquid film on the coating surface prior to impact) is important. Contrary to this, substrate curvature and the water nozzle-coating distance (< 10 cm) did not influence the results to any significant degree. The ranking of abrasion resistance of the blade coatings was in agreement with the ranking of rain erosion resistance measured in the whirling arm rig and is an interesting indication for future work.

Finally, in chapter 4, conclusions are drawn and suggestions for further work provided.

Dansk Resumé (Summary in Danish)

Under drift udsættes de hurtigt roterende vinger på vindmøller for gentagne kollisioner med regndråber, hagl, insekter eller partikler. Det kan føre til erosion af vingerne, hvilket går udover den elektriske effektivitet, og dyre reparationer kan blive nødvendige. En mulig løsning på dette problem er elastiske vingecoatings, der er i stand til at absorbere kollisionsenergien uden at revner eller andre skader dannes. Formålet med arbejdet, der præsenteres i denne afhandling, har været at designe og konstruere en eksperimentel laboratorieopstilling, der muliggør en accelereret og pålidelig evaluering af eksisterende og nye vingecoatings-formuleringer. Resultater fra eksperimenterne sammenlignes med data fra den større "roterende arm" opstilling (på engelsk *whirling arm*), der er den nuværende industrielle standard til evaluering af vingecoatings. Den "roterende arm" opstilling består af tre hurtigt drejende horisontale rotorer, der bevæger sig igennem et kraftigt, kunstigt pålagt, "regnvejr".

Afhandlingen indeholder fire kapitler. I kapitel 1 gives i et litteraturstudium baggrundsinformation om området. Emner, der diskuteres er den globale vindenergiudvikling, mulige vindmølle konstruktioner, vingestrukturer og -materialer, vingecoatings og mekanismer for væskeerosion. I kapitel 2 beskrives design, konstruktion og evaluering af en ny laboratorieopstilling til hurtig simultan screening af 22 coatingsprøver. Apparatet er baseret på et princip med diskrete vandstråler. En gennemgang af tidligere forsøgsudstyr til test af regnerosion er også inkluderet.

For at give basis for sammenligning af den nye opstilling med den "roterende arm" opstilling, blev en dimensionsanalyse samt eksperimenter med to polyurethan-baserede vingecoatings udført. Resultater viste, at vandstrålehastighed og kollisionsfrekvens er de vigtigste parametre for erosionshastigheden af coatings. Ydermere lader det til, at meget små defekter i coatingoverfladen, der ofte er til stede i de testede enheder, spiller en betydelig rolle for erosionsmekanismen. Evalueringen af coatings, under forhold hvor kollisionsfrekvens og vandhammertryk var "bevaret", kunne ikke direkte korreleres med resultater opnået med den "roterende arm" opstilling. Blandt andre medvirkende faktorer kan det muligvis tilskrives forskellige kontaktformer i de to opstillinger, dvs. bevægelse af coatede paneler mod regndråber, kontra bevægelse af vanddråber mod coatede paneler. Resultaterne viser den komplekse natur af regnerosionsfænomenet, der er en konsekvens af simultan

kombination af komplekse mekanismer, som derfor er vanskelige at reproducere i laboratorieskala.

I kapitel 3 blev den eksperimentelle undersøgelse udvidet med et studie af effekter af tre vigtige procesparametre på coatingserosion: vandafbødning, substratkrumning, og afstanden mellem vanddyse og coating overflade. Ydermere, for at kortlægge indflydelsen af fysiske egenskaber på regnerosion, blev der udført mekaniske målinger til karakterisering af udvalgte vingecoatings. De mekaniske målinger inkluderer elasticitetsstyrke-, kollisions-, hårdheds- og slidstyrkeeksperimenter. Undersøgelserne viste, at i nogle tilfælde er vandafbødning (tilstedeværelsen af en væskefilm på coatingoverfladen inden kollisionen) vigtig. Derimod påvirkede substratkrumning og afstanden mellem vanddyse og coating (<10 cm) ikke resultaterne i væsentlig grad. Rangering af slidstyrke af vingecoatings var i god overensstemmelse med ranglisten for regnerosionsstyrken målt i den "roterenede arm" opstilling, hvilket er en interessant indikation for fremtidigt arbejde.

I kapitel 4 drages der afslutningsvis konklusioner samt gives forslag til fremtidigt arbejde.

Table of Contents

Chapter 1 - Literature survey on wind turbines, liquid erosion, and blade coatings

1.1 Introduction

Energy resources can be classified into three categories: fossil fuels, renewable resources, and nuclear resources. Fossil fuels are at present the dominant energy source, especially coal, oil and natural gas. Fossil fuels supplied about 78% of global electricity production in 2013 as shown in Figure 1.1.
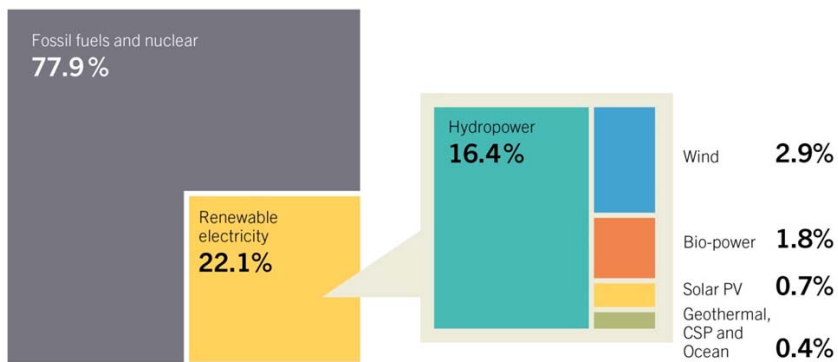
Figure 1.1 Estimated renewable energy share of global electricity production by the end of 2013. Solar PV is solar photovoltaic. CSP is the concentrated solar power. Reproduced from [1].

The reserves of fossil fuels are limited and their large-scale use is associated with environmental issues such as acid precipitation, stratospheric ozone depletion, and the global climate change. The results have been a rapid growth in the level of greenhouse gas concentration in the atmosphere and an increase in fuel prices, which are the main driving forces behind efforts to utilize renewable energy sources [2].

Renewable energy sources include biomass, biofuels, solar radiation, wind, hydropower, and geothermal energies. About 22% of the global electricity was in 2013 generated by renewable energy (Figure 1.1) [1].

Wind energy is attracting global interest. Figure 1.2 shows its growth in the last 18 years. The installed worldwide wind capacity has increased dramatically in the last decade, and reached 318,137 MW in the year 2013 [3]. Wind energy presently covers around 0.2% of the total global energy demand and only 1.8% of the world's

electricity is being generated by wind energy. The latter is by far the most efficient and most clean of all the known renewable energies, and is expected to lead the shift from fossil fuels to renewable energies [4].
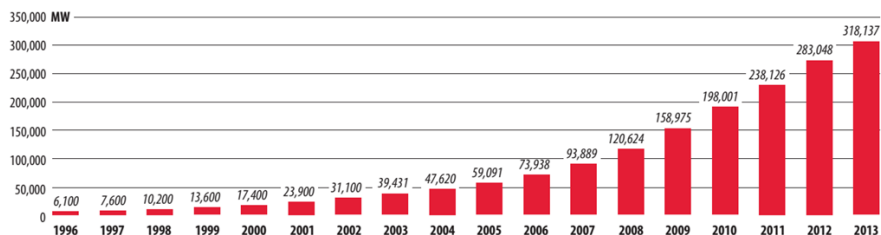
Figure 1.2 Global cumulative installed wind capacity 1996-2013. Reproduced from [3].

For many years, the wind industry has been driven by five big markets: China, USA, Germany, Spain, and India. These countries have had the largest shares of wind power during the last two decades. In 2012, they represented 207 GW, or 73 % of the worldwide wind capacity [5]. Denmark is the leader in terms of installed wind power capacity per person; the country has an installed wind capacity of 752 W per person in 2012. Spain, Portugal, Sweden, Germany, and Ireland rank in the top ten. The USA ranks 12, with close to 200 W per person, and China ranks 36, with 56 Watt per person, both far behind their absolute position but still above world average. India is at position 52 with 15 W per person, below the global average. If all countries had the same density like today Germany or Denmark, the world would see a total installed capacity of 12,000,000 MW, more than enough to cover the world's complete electricity demand. There is still a huge potential to harvest wind power [5].

The remaining of this chapter will provide insights into the wind turbine, wind turbine blade structure, materials and coatings, leading edge blade erosion, and material degradation mechanisms.

1.2 Wind turbines

Wind turbines convert the kinetic energy of wind into mechanical power and a generator converts it into electricity. The use of wind turbines to generate electricity began with a few technical innovations such as the use of synthetic materials to build rotor blades, and continued with developments in the field of aerodynamics,

mechanical and electrical engineering, and control technology. Electronics provided the technical basis for wind turbines commonly used today. Since 1980, wind power has been the fastest growing energy technology in the world [6].

There are two main types of wind turbines, the horizontal axis wind turbines (HAWTs) and vertical axis wind turbines (VAWTs). The main types of wind turbines are shown in Figure 1.3.
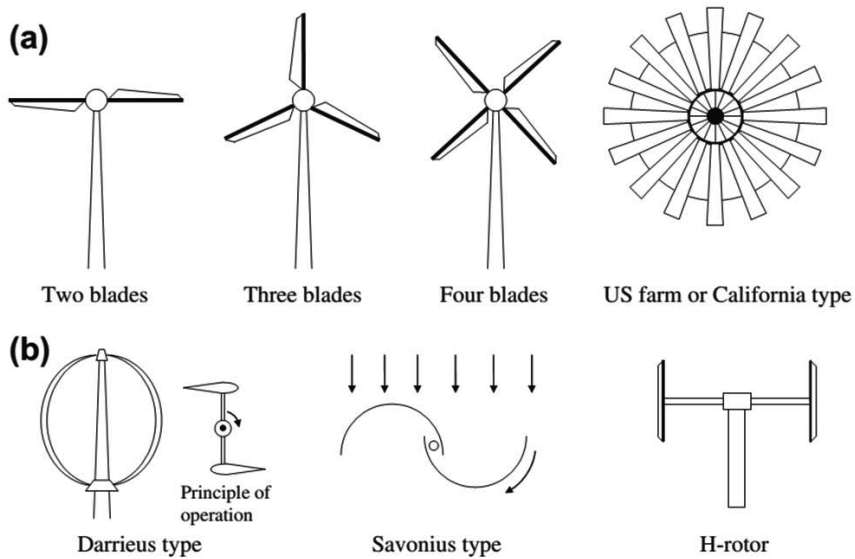
Figure 1.3 Wind turbine configurations. (a) Horizontal axis wind turbines. (b) Vertical axis wind turbines. Reproduced from [7].

Most modern wind turbines have a horizontal axis with blades resembling airplane propellers. Horizontal-axis units account for almost all utility-scale turbines, for example, 100 kilowatts or several megawatts [5]. The most feasible design offering the lowest cost is the two-blade type. However, the major drawback of both one and two blade designs is the high level of noise generated [4]. It was found that the three-blade rotor is the most efficient for power generation by large wind turbines compared to all the other turbine types. It allows for a better distribution of mass, which makes rotation smoother with lower noise and an acceptable cost. The alternative is the VAWTs. Their weight is supported by a ground level bearing and both the gearbox and the generator can be at ground level, which makes maintenance easier compared to HAWTs. Vertical-axis machines are good for pumping water and other high torque low-speed applications and are usually not connected to the electric power grid. The

3

blades of VAWTs are susceptible to resonant vibration and have lower efficiencies [7, 8].

Wind turbines are considered a mature technology and are provided commercially in a wide range of capacities from 400 W to 7.5 MW [9]. The theoretical maximum aerodynamic conversion efficiency of wind turbines from wind to mechanical power is 59%. However, the peak efficiency is about 45% in practice. The average annual efficiency of most turbines is about half this number. This is due to the need to shut down the wind turbine in low or high winds and to limit the power once the rated level is reached. It may also be caused by generator loss and the fact that the machine does not always operate in its optimum working point [7].

To reduce the cost of energy production, manufacturers have increasingly sought to increase the size of turbines. For a given wind speed, the mass of a turbine is approximately proportional to the cube of its blade-length. Wind power intercepted by the turbine is proportional to the square of its blade-length [9]. The growth in size of wind turbines since 1980 and prospects is shown in Figure 1.4. The largest units today can produce 7.5 MW and have a rotor diameter of 170 m. It is anticipated that turbines with diameters of 250 m capable of producing 20 MW will be produced in the coming years. These are possible today after the recent developments in carbon fiber reinforced blade production, which allows the manufacture of long and strong blades with less weight [7].
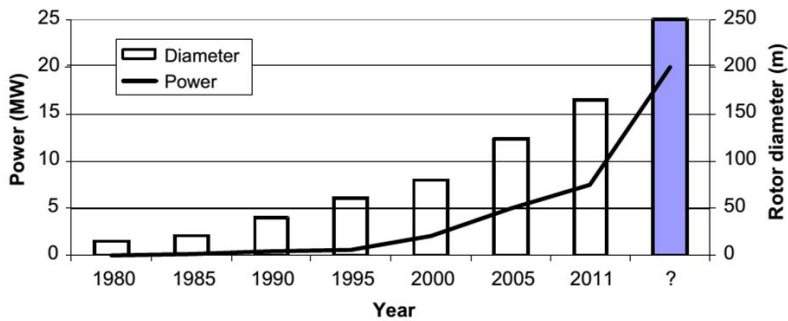
Figure 1.4 Growth in size and power of wind turbines since 1980 and prospects. Reproduced from [7].

As shown in Figure 1.5, there is a slight trend in increasing tip speed with increasing rotor diameter with the increase of blade length, the blade tip speeds can be as high as 100 m/s.
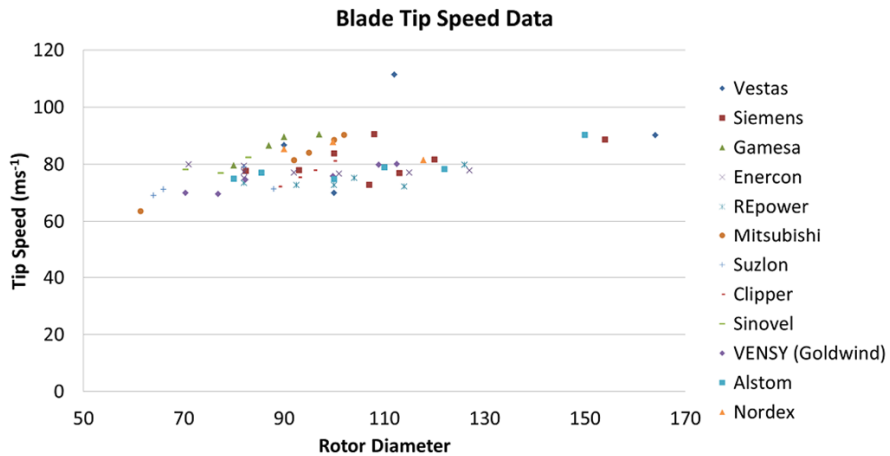
Figure 1.5 Blade tip speed versus rotor diameter for various utility scale wind turbine blades. Reproduced from [10].

It should also be noticed that the tip speed only represents the maximum possible values; the blades may only operate at these speeds for a limited time. However, these high speeds can cause erosion much faster than the slow speeds. Advanced blade materials and blade coatings are required to survive 20 years life span under those new challenging conditions [11].

During continuous operation, the blades are not only exposed to different environmental factors, but also to constant fatigue loading. Additionally, during this period, the frequency of maintenance and access to the blades has to be kept at a minimum to reduce the production and financial losses associated with turbine down time [10].

1.3 Blade structure and materials

The maximum blade length of a turbine is limited by both the strength and stiffness of its material. There is a need to develop stronger and lighter composite materials. To reduce material cost and weight, the blade is hollow in the middle. The blades are subject to a wide range of loads including flapping, tension, compression and twisting, and must be stiff enough to avoid impacting the towers. The stiffness is determined by both the internal structure and material of the blade [8, 12]. One of the blade structures is shown in Figure 1.6.
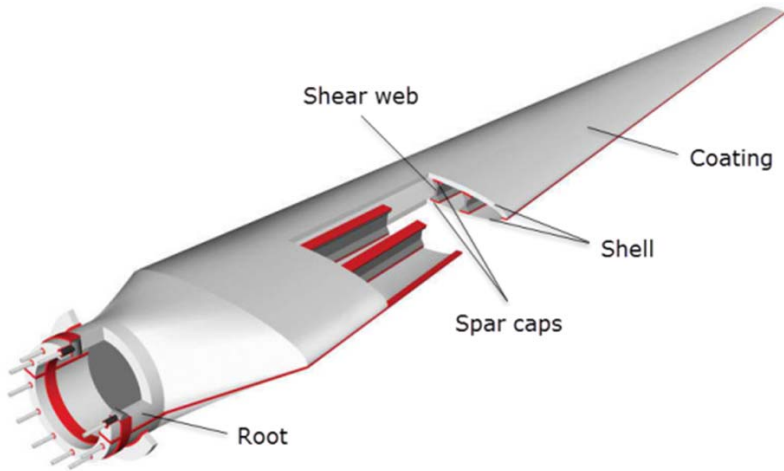
Figure 1.6 Wind turbine blade structure. The root is for connecting with wind turbine hub. The shell is to provide the aerodynamic shape and a structural role in stiffness and strength. The shear web and spar caps form the spar enhancing structure strength of a blade. The coating is for protecting the blade from environmental threats such as UV radiation and impacts from foreign bodies. Reproduced from [13].

The high material stiffness is also needed to maintain optimal aerodynamic performance. A low density is needed to reduce gravity forces and long fatigue life is needed to reduce material degradation [14]. The majority of wind turbine blades use composite materials of thermosetting polymer matrix reinforced with fibers. The glass fiber, having a good combination of stiffness, strength and density, has been used since the early days of blade manufacturing. Carbon fibers are now attracting attention due to their superior mechanical properties compared with glass fiber and decreasing price. Other potentially interesting fibers are aramid, polyethylene, and cellulose, all of which have moderate mechanical properties, and low or very low densities [14]. Different fibers can also be mixed to achieve the required stiffness, strength, and weight. Fibers are used in various forms to support different structures [14]. These materials, compared with conventional structural materials such as steel and wood, exhibit characteristics such as low density, stiffness, and high strength, good anticorrosion properties, fatigue resistant, and low manufacturing cost [8, 15].

The polymeric matrix also plays an important role in the composites, supporting the fibers and bonding them together. The fibers must be kept in the desired orientation, so the composite can satisfy the structural purpose. The matrix resins most commonly used can be divided into three major classes: polyester, epoxy and vinyl ester. The

6

resulting composite materials are commonly referred to as glass-reinforced plastic (GFRP) and carbon fiber-reinforced plastic (CFRP). Blades made of wood or hybrid of wood and carbon fibers are normally impregnated with epoxy resin [8]. Reinforced thermoplastics offer significant advantages over thermosets when used to produce recyclable rotor blades for utility-scale wind turbines. At the end of service life, thermoplastic blades can be recycled by heating and forming them into something else. Thermoplastics for composites for rotor blades have been under development for the past 10-15 years [16]. The composite properties are generally governed by the fibers, the matrix and the interface between these components. The general requirements for future composites used in wind turbine blades are enhanced mechanical properties especially stiffness and fatigue, improved processing time, low cost as conventional fabrics, and improved reliability [15, 17].

1.4 Leading edge erosion phenomenon

Composite wind turbine blades are designed to last for about 20 years in the field. However, the composite materials are susceptible to heat, moisture, UV radiation, and erosion from both solid particles and rain. They also suffer from impacts with wild life such as birds and insects [10, 11]. These influencing factors will deteriorate or contaminate surface coatings. The early roughness created can increase the extent of transitional flow as well as increasing turbulence intensity near the wall. The roughness size, density and location are the most important parameters influencing wind turbine performance, which tends to decrease with increasing roughness size and density [18, 19]. The most susceptible part of a blade is at the tip, where the speed is the highest. Evidence of this was e.g. seen on an investigation of an 11.6 m length DEBRA-25 wind turbine blade after almost 20 years of operation [20].

Depending on operating conditions, erosion of rotor blade leading edges (Figure 1.7) can affect wind turbine energy generation efficiency.

Figure 1.7 Leading edge erosion of a wind turbine blade. Reproduced from [21].

Erosion can happen as soon as two years after installation [10, 22]. The erosion process on wind turbine blades typically starts with the formation of small pits or from small tears or scratches in the leading edge which may act as initiation sites for further erosion. The defects will increase in size and density over time and combine to cause delamination of the leading edge [19, 21]. If repairs are not done early, damage to the underlying laminate will be present as early as after five years. It was found that a polyester resin exhibited a decrease of 15% in average failure strain, a decrease of 30% in ultimate strength and an 18% decrease in tensile modulus after exposed to moisture and UV light. Carbon reinforced epoxy composite under UV exposure resulted in a 29% reduction in the transverse tensile strength [10]. If these failures are not repaired there is potential for imbalance in the blade set, strain on the nacelle, and the additional wear being exerted on the bearing. There is also the additional potential for loss in blade stiffness and the risk of a catastrophic failure caused by impact with the tower [11]. If water enters the core material of the blade, the core expands and contracts as the freeze-thaw cycles occur and the core will separate from the laminate. When a blade is damaged at this level, the blade must be brought to the ground to be repaired, which will cost a minimum of 75,000 US dollars per set, or new blades have to be purchased, which will be even more expensive [21]. In fact, every defect on the surface of a wind blade disrupts its aerodynamic efficiency and, as a result, reduces the power production of the turbine. Researches have shown that leading edge erosion can produce substantial airfoil performance degradation, yielding a large increase in drag coupled with a significant loss in lift near the upper corner of the drag polar (the relationship between the lift on an airfoil and its drag), which is critical for maximizing wind turbine energy production [19].

1.5 Coatings

In this section, a brief general introduction to coatings is provided. The following section deals more specifically with blade coatings. A coating is to provide surface protection, decorative finishes and numerous special functions for commodities and merchandise formulated with organic and/or inorganic chemicals. The liquid coating materials contain the same basic compositional components: resin, solvents, pigments and additives [23, 24].

1.5.1 Resins

The resin is the most important component of the coating and is responsible for providing substrate adhesion, binding the pigment, and for ensuring the right chemical and physical properties [23]. The resins can be made from natural oils. However, most of the resins are synthetic organic polymers such as epoxies, urethanes, vinyls, and alkyds [24]. Thermoplastic coatings are formed from high molecular weight polymers drying physically by the evaporation of solvents. An increase in the molecular mass of the binder in the polymer film improves properties such as elasticity, hardness and impact deformation. Chemically cured thermoset coatings are formed by a chemical reaction between a resin reactant and a crosslinker or curing agent [25].

1.5.2 Solvents

Solvents are used primarily to make application of the coating possible. In chemically curing systems, the volume of solvent also controls the reactivity of the system (potlife). Solvent systems are most often blends of different solvents, most of them are low molecular weight, organic chemicals [23].

1.5.3 Pigments

Most of the pigments are inorganic compounds such as oxides and silicates, many of the brighter colors are complex organic compounds. Pigments such as titanium dioxide, carbon black, and iron oxide add color and opacity to the paint. Pigments can also provide improved durability and weathering, corrosion resistance, antifouling or fire retardence [23, 26]. Extender pigments or fillers such as talc and clay cannot add opacity or color, but they can provide mechanical strength, gloss control, and pigment volume adjustment [23]. The shape of the pigments can be spherical or lamellar; they can give different barrier properties. The pigments have a big influence on the

viscosity of the coating. The desired coating properties are optimized with mixtures of pigments and other components [27].

1.5.4 Additives

The coating additives are auxiliary components added in low concentrations to improve specific properties. Catalysts are added to accelerate curing. Leveling agents are used to promote the formation of a smooth and uniform surface. Wetting agents consist of dispersants and anti-settling agents, they are used to reduce the surface tension between the binder solution and the pigment surface, they also aid wetting of the pigments and prevent flocculation of the pigment particles [24, 27].

1.6 Blade coatings

Wind turbine blade coatings, although accounting for a small part of total cost of a new wind turbine set, play an important role in mitigating leading edge erosion. The coating can protect the composite material from environmental factors such as UV radiation, moisture, and heat, and can also protect the composites from foreign body impacts. Many manufacturers offer protection in the form of a tape or a coating. The small increase in cost with leading edge protection is estimated to be worthwhile throughout the life of a wind turbine [21].

The high performance wind turbine blade coatings are becoming increasingly critical to wind farm operation over long periods with the use of larger blades. Wind turbine blades have to be repaired to keep them operating at maximum efficiency when erosion happens. With a growing number of blades now in service, blade maintenance is becoming a major issue. However, the repair is time consuming, and the down time reduces the revenue of wind farms [11, 28].

There are two ways to apply a surface coating. The first one is called the in-mould application. A surface coating layer is added to the surface of the blade as part of the molding process. For manufacturing reasons, the coating formed through this approach typically consists of a layer of material similar to that of the matrix material used in the substrate. The other method is called post-mould application; coatings are applied by painting or spraying. This approach allows more flexibility with materials; one common application is an elastic polyurethane material [10].

Epoxies and urethanes have been widely used in the protection of wind turbine blades; the emphasis continues to be on epoxies and polyurethanes nowadays, and

with a growing interest in waterborne formulations which is being driven by the need to meet increasingly strict environmental regulations [29]. The coating producer PPG has claimed that its thin film system with epoxy primers and polyurethane topcoat deliver long term, low maintenance asset protection in any operating environment including desert or offshore. The thin-film system provides protection with reduced film thickness, and therefore reduces VOC emissions, blade weight, cost and process time [30]. BASF has also claimed that its polyurethane compounds based topcoat exhibits high erosion resistance against rain, sand and hail. It can be used both onshore and offshore [31]. The material company 3M has developed a two component polyurethane tape coating that should provide erosion protection in a single layer. However, these tapes must be replaced frequently, otherwise they fail to adequately absorb the impact energy of the particulate matter. The tapes are suitable for small turbines because they can increase the aerodynamic drag on the blade surface [32]. The edges of polymeric tapes are also vulnerable to water impact, and tests have revealed de-bonding of tapes due to water droplets striking the edges of tapes, causing them to lift [33]. Similar to the wind turbine blades, aircrafts are also exposed to erosive environments. To protect the aircrafts in a similar way, most of the aerospace coatings systems also use epoxy as primer and polyurethane as topcoat.

Fluoropolymer-based coatings also have attractive properties for wind turbine blades. A company named "The 21st Century Coatings" has claimed that fluorinated coatings with low surface energy reduces the drag. Their products have proven field performance for over 15 years in harsh environments like desert climate, immersion, and urban areas with pollution, rain, snow, and heat. Although the coating may have attractive properties, fluoropolymer-based coatings are not yet used extensively in wind energy applications [29]. Waterbased hybrid resin technology has become commercially available by combining poly(vinylidene fluoride) (PVDF) copolymers and acrylic resins, and is regarded as a potential technology for use in wind turbine blade coatings. In the preliminary studies, evidence has been found that Taber abrasion resistance is improved by urethane crosslinking of PVDF hybrids [34].

Siloxane-based coatings are also claimed to exhibit good erosion resistance performance. A patent imparts an erosion-resistant coating composition comprising a cross linked epoxy polymer interpenetrated by a siloxane polymer. A good resilience (energy absorption) ensures erosion resistance and was achieved by the long linear siloxane segments present in sufficient quantity, obtained by silanes having two

hydrolysable groups per silicon. With hard particles such as diamond, alumina and silica incorporated, the composite will provide strength and resistance to abrasion [35]. Karl Erik Wiedemann et al. patented a simple formulation comprising silanol fluid, fumed silica, solvent, catalyst, pigment, and silane as crosslinking agent. The coating can be applied directly on the metal substrate or an epoxy substrate and it is claimed that it can provide superior erosion resistance to glass-fiber reinforced epoxy, aluminum, nickel, stainless steel and polyurethane tape [36]. However, the use of fluoropolymer- and siloxane-based formulations for blade coatings is strongly limitted by their high material cost.

Another application is the use of nanocomposite layers to the leading edge of an airfoil. Nanocomposites form very high contact angles with water and the reinforced polymer acts to absorb and dissipate the impact energy from the repeated impacts of particulate matter. Reinforcing the polymeric network by nanoparticles with a certain diameter could increase the liquid impact resistance due to the increase of inorganic cross-linking, but this is not a universal rule to improve erosion resistance. It also depends on the synergistic effect with other groups. For example, higher organic content of the system can limit inorganic cross-linking of particle and matrix which will disturb the homogeneous network leading to surface defects that act as initial points for further erosion [37]. There exists a wide variety of nano-scale pigments based on titania, alumina, silica, clays and carbon nanotubes. The coating properties depend strongly on the geometry of the pigments [33]. A nanocomposite coating technology roadmap is shown in Figure 1.8.
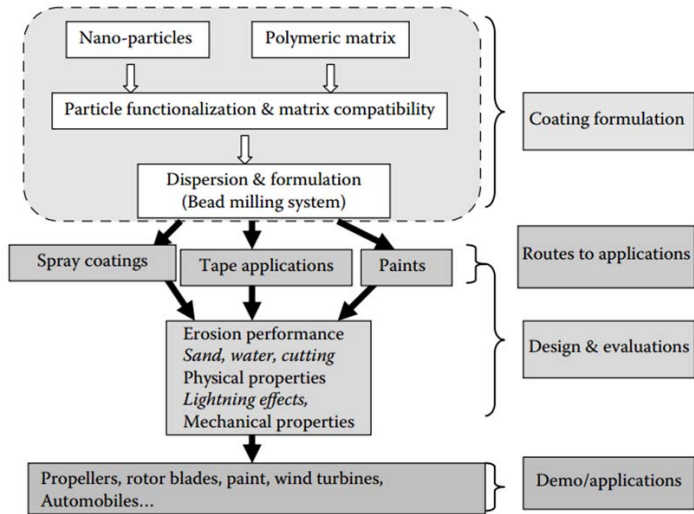
Figure 1.8 A proposed nanocomposite coating technology roadmap. Reproduced from [33].

1.7 Liquid erosion

Investigations into the material aspects of steam turbine blade erosion (Figure 1.9) began in the early 20th century when the tip velocities of the blades of steam turbines became high enough to cause erosion [38].
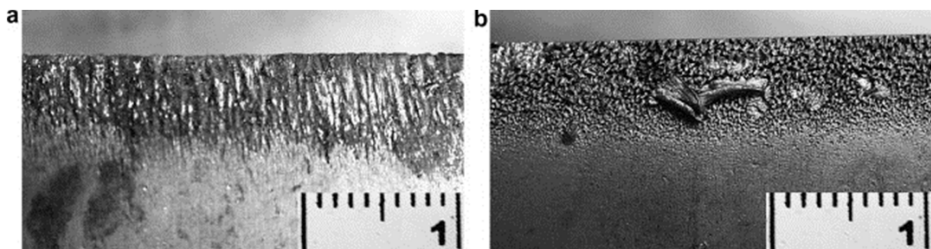
Figure 1.9 Steam turbine blade erosion. Reproduced from [39].

Rain erosion became a problem in the 1940s. It was noticed that plastic, glass, ceramic and even metallic surfaces of an aircraft could be damaged when flying through heavy rain [40]. Droplets impinging at a high speed onto the surface of a solid can exert forces of a magnitude sufficient to permanently deform and fracture the solid. The erosion is a complicated process and the type and extent of the erosion

damage depends on a number of factors from both liquids and the solid materials [40, 41].

1.7.1 Effect of impact variables

1.7.1.1 Impact velocity

There have been many attempts to discover a general relationship between impact velocity of water droplets and erosion damage which could be valid for a wide range of materials. Presently there is no such numerical relationship which can be applied to materials other than those to which the measurements refer. In general, as the impact velocity is increased, the erosion is also increased [42].

1.7.1.2 Drop size and shape

Large drops can cause erosion at considerably smaller velocities than those required for small drops. Large drops cause faster erosion damage due to the larger hammer pressure on the surface and the possibility of varying the pressure distribution over the impacted area [40, 42]. However, Gohardini claims that damages due to an impacting water drop are strongly dependent on the radius of curvature at the point of contact and not so much the mass of a distorted water drop. Distorted drops with radii of curvature greater than their initial diameters will therefore be proportionately more damaging [43].

1.7.1.3 Impact angle

A general conclusion is that the normal component of impact velocity of a droplet is mainly responsible for the damage (see Figure 1.10); the tangential component in most circumstances has little effect [38, 40]. However, for ceramics and hard polymers at high impact velocities, the tangential components may cause substantial damage of equal magnitude to the normal component [44].
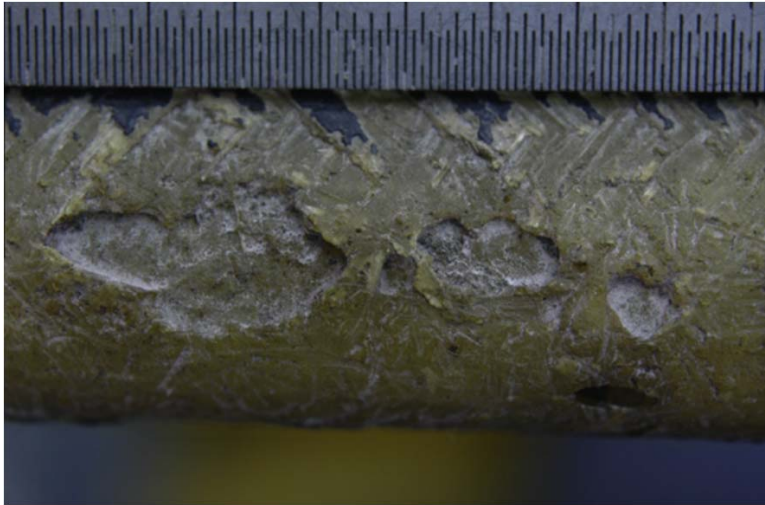
Figure 1.10 Erosion of the leading edge of a wind turbine blade removed from service. Leading edge dimensions shown are 44 mm horizontally and 20 mm vertically. Reproduced from [45].

1.7.1.4 Sample shape and roughness

Samples with different radii of curvature, from the airfoil shape to the planar, were investigated and it was found that the erosion rate increased when the impact surface was made concave [40]. However, research also shows that a plane surface was more rapidly eroded than a convex one. A slightly roughened surface will erode faster than a surface with less roughness [40, 42].

1.7.1.5 Wet surface

The liquid can be trapped in the bottom of pits formed on eroded surfaces. The trapped liquid will act as a cushion for oncoming impacts. The presence of a liquid film might also reduce erosion damage by cushioning the impact. When a wet surface is struck by a drop, the liquid film deforms and the pressure on the solid is less than it would have been if the surface was dry. Another explanation is that the impact pressure is reduced because the pressure wave diverges as it passes through the liquid layer [40, 42].

1.7.1.6 Temperature

The erosion rate will be affected by the temperature of the environment and the liquid drops. Experiments have shown that the erosion rate increases when the temperature

of the water increases. This might be due to the reduction in the viscosity of the liquid. As the viscosity increases, the velocity of the outward flowing liquid increases and the surface will experience more shear damage [38, 42].

1.7.2 Effect of material properties

Researchers have been searching for appropriate material properties to correlate with erosion resistance. There is relatively little correlation between the erosion resistance and macroscopic mechanical properties [41, 46]. Limited success in correlation with some of the material properties has been based on individual cases [47]. It is advocated in ASTM G73-10 that the erosion resistance should not be regarded as a precisely-definable property of a material, but rather as a complex mix of properties whose relative importance may differ depending on the variables of impacting conditions and materials [48]. For polymers, a large number of factors can affect the erosion resistance including the crystallinity, physical and chemical network characteristics, thermal conductivity, glass transition temperature, mechanical properties, such as hardness, tensile strength, modulus of elasticity, fracture toughness, yield stress, rebound resilience, friction coefficient, ultimate strength and elongation [32].

Materials with anti-erosive properties can be extremely hard and tough such that the impacting particle is unable to make any impression on the surface. However, highly elastic materials can also be used so that the kinetic energy of the particle is dissipated. Thus, no general statement for erosion properties of a polymer can be easily made without additional research focused on revealing the appropriate combination of properties necessary for a material to be truly anti-erosive [32]. The homogeneity of the surface is one of the important factors affecting resistance to rain erosion [49]. For the same resilient coatings, the thicker coatings can protect the adhesive bond between coating and substrate more effectively than thin coatings by stretching the coating to dissipate the stress [50]. A method of predicting the average period between raindrop impacts is illustrated in Figure 1.11. The upper curve shows an idealized series of applied stress pulses, spaced a period T apart. The lower curves compare the strain versus time of two different elastomeric coatings. Material A, which has a relaxation time, t_A, greater than the impact period T, does not have time to fully recover before the next impact. As a consequence, the successive impacts cause cumulative strain in Material A. The recovery of Material B, with t_B less than T,

is essentially complete after each impact. Therefore, after several impacts Material A has reached a strain $\Delta\varepsilon$ greater than Material B. The relation between relaxation time and impact period may be as important as the ability of the material to withstand a single impact [51].
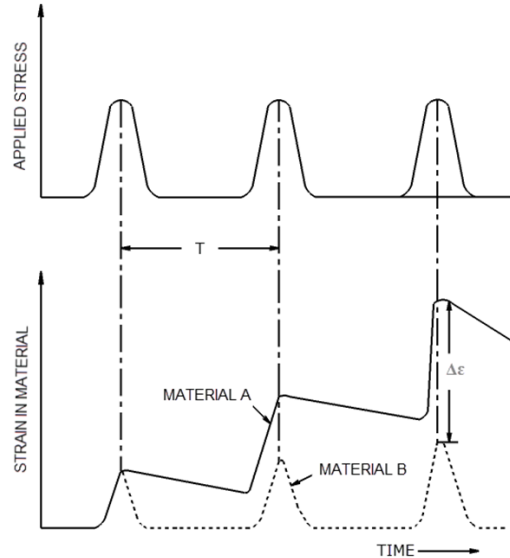
Figure 1.11 Relation between raindrop impact interval T and relaxation time, t, of elastomeric materials. After several impacts Material A, with $t_A > T$, reaches a strain $\Delta\varepsilon$ greater than Material B, with $t_B < T$ [51].

1.7.3 Liquid erosion mechanism

During a high velocity impact of a liquid drop on a solid target, high pressure develops at the interface between the solid and liquid. The pressure generates stress waves. Consequently, intensive stress produces damage at local sites [52].

When a water drop impacts a plane rigid surface, the overall impact sequence can be divided into two phases: the pressure build-up phase prior to fully develop lateral outflow jetting and the pressure release phase as the drop collapses onto the surface. As shown in Figure 1.12, at the initial stage of the impact, the contact edge travels across the surface of the target at a velocity, V_C, which is greater than the shock wave velocity propagating into the water drop. The water behind the shock front is compressed because there are no free surfaces for the pressure release [37].
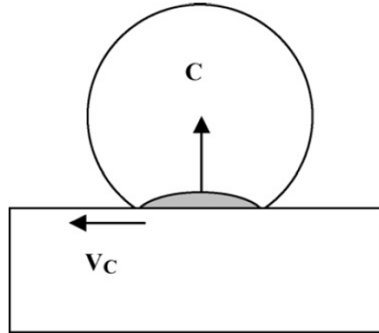
Figure 1.12 Droplet after initial impact: water drop is compressed due to lack of a free surface. V_C is the contact edge velocity. C is the shock wave velocity. Reproduced from [37].

The pressure exerted on the surface of a rigid target is known as the water hammer pressure, P, which is given by

$$P = \rho_0 C_0 V \qquad (1)$$

where ρ_0 is the density of the liquid, C_0 is the acoustic wave velocity in the liquid, and V is the liquid impact velocity. The water hammer pressure is one dimensional, representing the impact between the planar surface of a semiinfinite liquid body striking a semiinfinite rigid body. No account is taken of the geometry of the impacting mass on the characteristics of the compression wave propagating into the liquid. The water hammer pressure is responsible for most of the damage resulting from liquid impact [41].

As illustrated in Figure 1.13, when the shock envelope overtakes the contact edge, a free surface is generated which allows the compressed region to release.
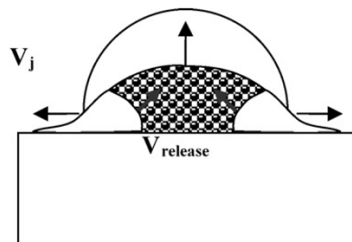
Figure 1.13 Droplet after shock wave has over-taken contact edge allowing decompression and jetting. V_j is jetting velocity. $V_{release}$ is the release wave velocity. Reproduced from [37].

The release waves propagate into the water drop from the free surfaces, reducing the pressure which is approximately the incompressible Bernoulli pressure P_i [37]

$$P_i = \frac{\rho_0 V^2}{2} \tag{2}$$

Lateral jets are produced in a second step of impact causing shear stress (Figure 1.14). The contact edge between the target surfaces slows down and is overtaken by the shock front. Thus, water trapped in the compressed region can escape which generates water jets across the surface causing a high velocity sideways jet of fluid. This fluid has a velocity V_j which is faster than the impact velocity V [37].

Figure 1.14 Damage effects of lateral jetting [37].

Lateral outflow jetting will not contribute to the initiation or extension of damage unless there is a preexisting surface irregularity with which it can interact [41, 52]. Hydraulic penetration of the water in a drop impacting over a preexisting crack or erosion pit is the most damaging mode for material removal, since it has the capacity to propagate submicrometer size crack and surface pits to measurable dimensions, on the order of several millimeters, and is effective throughout the material removal process [41].

The actual mechanism of material removal is a complicated series of interactions between an impacting water drop and the changing material surface, and possibly involving all of the mechanisms mentioned above. Failure modes inherent in the target material are intimately associated to the damage process. It is therefore difficult to establish a clear connection between the overall dynamics of the impact process and the erosion response of the material. More details in terms of interactions between pressure waves can be found in Chapter 3.

The rate of erosion due to liquid impact is not constant with time, but exhibits several erosion rate-time patterns. In the ASTM G73-10, four stages corresponding to incubation period, accelerating stage, steady-state, and the decelerating stage are defined. The most common mass loss/exposure curve is shown in Figure 1.15.
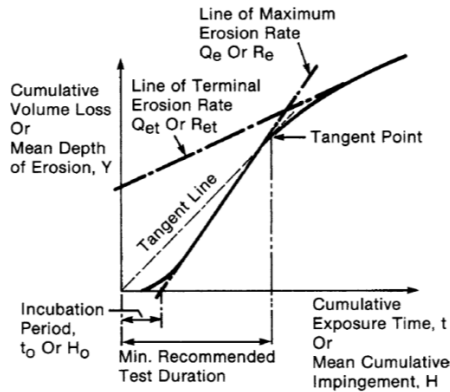
Figure 1.15 Cumulative erosion-time curve. Reproduced from [48].

There is an initial period, the incubation period, during which there is a slight or an absence of material loss, although there will usually be some plastic or brittle deformation of the surface. During the next period, material is removed at an accelerated rate until a maximum rate, after a time, the erosion rate begins to decrease, tending to a lower and approximately constant rate [38, 40]. However, the actual pattern varies with the conditions of impact and the material. The significance of the various stages can differ according to the intended service applications of the materials being tested. In most practical situations, the initial three periods are of concern. The major problem centers on events taking place during the incubation period, and improvements in material performance are accomplished by modifying the material to extend the incubation period [41]. The incubation time is the most important for coatings because service life is usually terminated by initial surface damage even though the mass loss is very limited [48].

1.7.4 Liquid erosion of various materials

One critical aspect that seems to be a common cause for the failure of existing polymeric coatings is surface shearing as the water droplet is deflected outward across the surface following normal impact. This can cause a radial pattern of deformation. Another aspect is penetration of water into tiny surface defects. Surface shearing could eventually cause surface defects due to tearing and fatigue cracking which can then be penetrated by the water, causing a rapid failure of the coating [33, 53]. At high speeds, water droplets have been shown to behave like hammers, which also

opens the possibility of impact induced de-bonding of the coating from the substrate, increasing the likelihood of tearing and fatigue damage. The substrate could also be damaged due to the transmission of pressure pulses with coatings left undamaged [33, 54]. The polymers must resist formation of cracks as a consequence of fatigue in repetitive yielding under random impacts of rain [47].

Low modulus or high resilience coatings such as elastomers will reduce the stress at the impact surface and thereby reduce the stress in the coating. These materials need to have mechanical strength with sufficiently high value to withstand the shear stresses of a single impact but also recover fast enough to be able to absorb the stresses of additional impact [52]. Therefore the recovery time and frequency of impact are important parameters since elastomeric materials are sensitive to multiple impingement effects [52, 54]. The attenuation of the impact stress wave will increase with coating thickness owing to the increased damping capacity of the material and the possible divergence of the stress wave so that there is a loss in the energy density before the wave arrives at the substrate [52]. In addition, the material must not lose its ability to absorb repeated impact stresses over long periods of exposure [50].

The void content and type of reinforcement in elastomeric coatings are shown to influence the behavior of fiber reinforced composite structure. The addition of reinforcement to thermoplastics is detrimental to erosion performance because the fibers tend to break out under repeated impingement enhancing the mass loss. The thermosetting polymers benefit from reinforcement because the fibers reduce massive breakage and chunking of the brittle resin [47].

Ductile materials such as most metals and thermoplastic polymers exhibit non-brittle behavior of surface depressions with upraised edges. These edges are susceptible to the lateral outflow jetting from the impacting drop leading to erosion pit nucleation [47]. Corrosion can be observed when steel is eroded by water [55], the combined erosion-corrosion process may have different failure mechanism compared with pure liquid erosion process. A high modulus metal coating on a composite is known to reduce the transmitted stress because it only transmits a very low stress pulse to the substrate [54].

Hard, rigid materials such as ceramic, glasses, uncoated composite and thermosetting plastics cannot mitigate to any notable degree, the impact and shear stresses that the colliding drop exerts. The response of rigid materials to liquid impact is typically cracking due to the direct deformation [47]. To have erosion resistance, rigid

materials must be able to withstand these combined stresses. The fracture or yield strength dominates the ability to withstand the unmitigated stresses [50].

1.8 Conclusions

Wind energy is one of the most promising renewable energy sources. Continued fast growth is anticipated and wind turbines with larger blades will be produced. This requires higher performance blade coatings to resist the more severe rain erosion environment. Erosion mechanisms have been studied in the past 100 years; however, due to the complex interaction in the erosion process, few correlations have been developed to help the production of more erosion-resistant materials. High performance blade coatings may prolong the life time of the blades and improve or maintain the electricity production. The ultimate target is to find the erosion mechanisms of elastic polymeric coatings when they are exposed to rain droplets. It seems worthwhile to invest time and resources in this area.

In the remaining part of this thesis, two studies are presented. In Chapter 2, a novel water jet based erosion test rig for fast screening of wind turbine blade coatings is presented and analyzed. In Chapter 3, evaluation of the erosion performance of the water jet rig continued by changing the erosion parameters such as water cushioning, sample geometry and impact distance. Tensile strength, flexibility, impact, hardness and abrasion experiments were conducted to characterize the coatings. Finally, in Chapter 4, conclusions are drawn and suggestions for further work provided.

Nomenclature

C	shock wave velocity
C_0	acoustic wave velocity in the liquid
P	water hammer pressure
P_i	Bernoulli pressure
T	raindrop impact interval
t_A	relaxation time of material A
t_B	relaxation time of material B
V	droplet impact velocity
V_C	contact edge velocity
V_j	jetting velocity
$V_{release}$	release wave velocity

Greek

$\Delta\varepsilon$	strain of material A
ρ_0	density of the impact liquid

References for chapter 1

[1] REN21. 2014. Renewables 2014 Global Status Report (Paris: REN21 Secretariat). ISBN 978-3-9815934-2-6.

[2] G.S. Alemán-Nava, V.H. Casiano-Flores, D.L. Cárdenas-Chávez, R. Díaz-Chavez, N. Scarlat, J. Mahlknecht, J. Dallemand, R. Parra, Renewable energy research progress in Mexico: A review, Renewable and Sustainable Energy Reviews. 32 (2014) 140-153.

[3] Global wind statistics 2013, note published by Global wind energy council (2014) 1-4, Brussels, Belgium.

[4] Tabassum-Abbasi, M. Premalatha, T. Abbasi, S.A. Abbasi, Wind energy: Increasing deployment, rising environmental concerns, Renewable and Sustainable Energy Reviews. 31 (2014) 270-288.

[5] S. Gsänger, J.D. Pitteloud, World Wind Energy Annual Report 2012, World Wind Energy Association (www.wwindea.org), (2013) 1-19, Bonn, Germany.

[6] M.G. Molina, J.M.G. Alvarez, Technical and regulatory exigencies for grid connection of wind generation, Wind farm (2011) 1-30.

[7] S.A. Kalogirou, Chapter 13 - Wind Energy Systems, in: S.A. Kalogirou (Ed.), Solar Energy Engineering (Second Edition), Academic Press, Boston, 2014, 735-762.

[8] B. Hayman, J. Wedel-Heinen, P. Brøndsted, Materials challenges in present and future wind energy, MRS Bulletin. 33 (2008) 343-353.

[9] Technology roadmap of wind energy 2013 edition, International Energy Agency (2013) 1-58, Paris, France.

[10] M.H. Keegan, D.H. Nash, M.M. Stack, On erosion issues associated with the leading edge of wind turbine blades, J. Phys. D. 46 (2013) 1-20.

[11] D. Cripps, The future of blade repair, Reinforced Plastics. 55 (2011) 28-32.

[12] P. Hogg, Wind turbine blade materials, http://www. supergen-wind. org. uk/presentations. html (Accessed 15.07. 2014).

[13] P. Roth-Johnson, R.E. Wirz, E. Lin, Structural design of spars for 100-m biplane wind turbine blades, Renewable Energy. 71 (2014) 133-155.

[14] P. Brøndsted, H. Lilholt, A. Lystrup, Composite materials for wind power turbine blades, Annu. Rev. Mater. Res. 35 (2005) 505-538.

[15] J. Zangenberg, P. Brøndsted, M. Koefoed, Design of a fibrous composite preform for wind turbine rotor blades, Mater Des. 56 (2014) 635-641.

[16] G. Marsh, Could thermoplastics be the answer for utility-scale wind turbine blades?, Reinforced Plastics. 54 (2010) 31-35.

[17] J.G. McGowan, R.W. Hyers, K.L. Sullivan, J.F. Manwell, S.V. Nair, B. McNiff, B.C. Syrett, A review of materials degradation in utility scale wind turbines, Energy Materials. 2 (2007) 41-46.

[18] E. Sagol, M. Reggio, A. Ilinca, Issues concerning roughness on wind turbine blades, Renewable and Sustainable Energy Reviews. 23 (2013) 514-525.

[19] A. Sareen, C.A. Sapre, M.S. Selig, Effects of leading edge erosion on wind turbine blade performance, Wind Energy (2013), John Wiley & Sons, Ltd. DOI: 10.1002/we

[20] F. Sayer, F. Bürkner, B. Buchholz, M. Strobel, A.M. van Wingerde, H. Busmann, H. Seifert, Influence of a wind turbine service life on the mechanical properties of the material and the blade, Wind Energy. 16 (2013) 163-174.

[21] L. Rampel, Rotor blade leading edge erosion – real life experiences, Wind Systems Magazine (Issue date 24.10.2012) 22-24.

[22] K. Wood, Blade repair: Closing the maintenance gap, Compos. Technol. (2011). http://www.compositesworld.com/articles/blade-repair-closing-the-maintenance-gap, (Accessed on 29.08.2014).

[23] C.H. Hare (Ed.), Protective Coatings - Fundamentals of Chemistry and Composition, SSPC 94-17 ed., The Society for Protective Coatings, Pittsburgh, USA, 1994.

[24] A. Goldschmidt, H.J. Streitberger (Eds.), BASF handbook on basics of coating technology, 2nd edition, Vincentz Network, Hannover, Germany, 2007.

[25] R. Lambourne, T.A. Strivens (Eds.), Paint and Surface Coatings-Theory and Practice, 2nd edition, Woodhead, Cambridge, 1999.

[26] D. Stoye, W. Freitag (Eds.), Paints, Coatings and Solvents, second edition ed., Wiley-VCH, Germany, 1998.

[27] Ullmann's Encyclopedia of Industrial Chemistry, Revised 2002., Wiley-VCH Verlag GmbH&Co., 2002.

[28] G. Marsh, Meeting the challenge of wind turbine blade repair, Reinforced Plastics. 55 (2011) 32-36.

[29] C. Challener, Coatings critical for wind energy efficiency. http://www.thefreelibrary.com/Coatings+critical+for+wind+energy+efficiency.-a0218660845 (Accessed 15.07. 2014).

[30] http://www.ppg.com/corporate/ppgwind/products/Pages/default.aspx. (Accessed 10.04.2014).

[31] http://www.basf.com/group/corporate/wind-energy/en/microsites/wind-energy/technologies/blades (Accessed 10.04.2014).

[32] N. Dalili, A. Edrisy, R. Carriveau, A review of surface engineering issues critical to wind turbine performance, Renewable and Sustainable Energy Reviews. 13 (2009) 428-438.

[33] H.X. Peng, Polyurethane nanocomposite coatings for aeronautical applications, in: J.S. Leng, A.K. Lau (Eds.), multifunctional polymer nanocomposites, CRC press, Boca Raton; London; New york, 2011, 337-388.

[34] M. Durali, K. Wood, D. Battocchi, M. Halzenbeller, Current developments, European Coatings Journal. 10 (2011) 30-34.

[35] B.M. Sanders, K.E. Wiedemann, Composite coatings for imparting particle erosion resistance. US patent 2004/6706405 B2.

[36] K.E. Wiedemann, R. Sivakumar, B.M. Sanders, Erosion resistant silicone coatings. US patent 2004/0225079 A1.

[37] M. Grundwürmer, O. Nuyken, M. Meyer, J. Wehr, N. Schupp, Sol–gel derived erosion protection coatings against damage caused by liquid impact, Wear. 263 (2007) 318-329.

[38] M. Ahmad, M. Casey, N. Sürken, Experimental assessment of droplet impact erosion resistance of steam turbine blade materials, Wear. 267 (2009) 1605-1618.

[39] C.R.F. Azevedo, A. Sinátora, Erosion-fatigue of steam turbine blades, Eng. Failure Anal. 16 (2009) 2290-2303.

[40] J.H. Brunton, M.C. Rochester, Erosion of solid surfaces by the impact of liquid drops, in: C.M. Preece (Ed.), Treatise on materials science and technology, Academic press, New York, 1979, 186-248.

[41] W.F. Adler, The mechanics of liquid impact, in: C.M. Preece (Ed.), treatise on materials science and technology, Academic Press, New York, 1979, 127-185.

[42] O.G. Engel, Mechanism of rain erosion, Wright Air Development Center, USA. Report No. 53-192 (1953) 1-54.

[43] W.F. Adler, Particulate impact damage predictions, Wear. 186–187, Part 1 (1995) 35-44.

[44] O. Gohardani, Impact of erosion testing aspects on current and future flight conditions, Prog. Aerospace Sci. 47 (2011) 280-303.

[45] K. Gharali, D.A. Johnson, Numerical modeling of an S809 airfoil under dynamic stall, erosion and high reduced frequencies, Appl. Energy. 93 (2012) 45-52.

[46] W.F. Adler, Rain impact retrospective and vision for the future, Wear. 233–235 (1999) 25-38.

[47] F. George, J. Schmitt, Liquid and solid particle impact erosion, Air Force Materials Laboratory, USA. Report AFML-TR-79-4122 (1979) 1-74.

[48] Standard test metod for liquid impingement erosion using rotating apparatus, American Society for Testing and Materials. ASTM G73-10 (2010) 1-19.

[49] C.B. Reilly, M. Orchin, Preparation and properties of polyurethane coatings, J Ind Eng Chem. 48 (1956) 59-63.

[50] N.E. Wahl, Investigation of the phenomena of rain erosion at subsonic and supersonic speeds, Bell Aerosystems Company, New York. Report ML-TR-65-330 (1965) 1-55.

[51] A.F. Conn, A. Thiruvengadam, Dynamic response and adhesion failures of rain erosion resistant coatings, Journal of Materials. 5 (1970) 698-718.

[52] J. Zahavi, S. Nadiv, G.F. Schmitt Jr., Indirect damage in composite materials due to raindrop impact, Wear. 72 (1981) 305-313.

[53] W.F. Adler, J.W. Morris, N.E. Wahl, Supersonic rain and sand erosion research: characterization and development of erosion resistant materials. Air Force Materials Laboratory, USA. Report AFML-TR-72-85 (1972) 1-277.

[54] G.F. Schmitt, Materials parameters that govern the rain erosion behavior of polymeric coatings and composites at subsonic velocities, Air Force Materials Laboratory, USA. Report AFML-TR-71-197 (1971) 1-105.

[55] R. McGechaen, M.M. Stack, A study of raindrop erosion of steel and polymer based composites: application to wind turbines. Wear. ISSN 0043-1686 (Submitted).

Chapter 2 - Erosion of wind turbine blade coatings - Design and analysis of jet-based laboratory equipment for performance evaluation

This charpter was submitted with the title "Erosion of wind turbine blade coatings - Design and analysis of jet-based laboratory equipment for performance evaluation" to the journal Progress in Organic Coatings, April 2014. (authors Shizhong Zhang, Kim Dam-Johansen, Sten Nørkjær, Pablo L Bernad Jr., Søren Kiil)

2.1 Abstract

Driven by the growth of the wind power industry during the last decade, the size of wind turbines has grown considerably and single-turbine power can nowadays reach a capacity of 8 MW with rotor diameters exciding 160 m. Rain erosion is a considerable threat to the mechanical integrity of the blades in such equipment. To reduce expensive blade maintenance repairs and to avoid out-of-service periods, energy-absorbing blade coatings are required to protect rotor blades from rain erosion. In this work we describe the design, construction and evaluation of a laboratory setup for fast screening of up to 22 coating samples that is based on water jet slugs. Our objective is to study the effect of the parameters involved in the rain erosion process and to correlate our experimental results with data obtained with the complex and expensive whirling arm rig, which has become the industry standard method of test for rain erosion. Our results showed that water slug velocity and impact frequency are the most influential parameters in the coating erosion rate. Coating defects, often present on the specimens tested, appeared to play an important role in the erosion mechanism. Two particular experimental blade coatings were investigated using the proposed experimental design. The evaluation of the coatings under conditions where impact frequency and water hammer pressure were "matched" could not be directly correlated with the results obtained with the whirling arm rig. This result may be attributed, among other contributing factors, to the different contact modes in the two setups, i.e. the movement of coated panels against rain drops versus the movement of water drops against coated specimens. Additional factors that require further investigation are the specimen geometries and the potential significance of the presence of a thin water film on the coated surfaces.

Our results endorse the complex nature of the rain erosion phenomenon, which is the result of the simultaneous combination of complex mechanisms and as such, it is difficult to reproduce at the laboratory scale.

2.2 Introduction

Erosion of industrial materials by impacting water droplets is a well-known event. One of the first reports on this topic goes back to the 1920s, when the erosion of steam turbine blades by water droplets present in the wet steam was reported and investigated [1]. During the 1940s, with the development of the aeronautical industry, it was observed that exposure to rain was the origin of severe material damage. Rain erosion damage was particularly severe on the forward facing components of aircrafts such as leading edges, radomes and infrared-transmitting windows. Rain erosion in aircrafts has now been minimised or even eliminated by the use of metallic shields and polymeric coatings or tapes on the components susceptible to damage [2].

Likewise, blades in wind turbines are exposed to rain erosion. Research in this field is growing, driven by the rapid development of the wind power industry during the last 10-15 years. Global wind power capacity was larger than 282 GW in 2013, with over 45 GW installed in 2012 alone. The largest wind turbine industry is placed in China while Denmark leads the wind power generation capacity per capita. Driven by the market growth, the size of wind turbines has increased dramatically in recent years. Today turbines up to 8.0 MW and over 160 m rotor diameter are available, where the tip velocity of the blades can reach a linear speed of 100 m/s (360 km/h).

In the case of offshore wind turbines, blade erosion is particularly problematic; the repair or the replacement of blades is very costly. Due to seawater aerosols, blade erosion rates for offshore wind turbines are approximately twice as high as the rates observed on inland wind turbines.

As an example, over the past three years, more than 200 blades on 80 wind turbines have been repaired at the wind turbine park Horns Rev off Blåvands Huk in Denmark [3]. The wind turbines were put into operation in 2002. Repairs have also taken place at other wind turbine parks: in Denmark at Rødsand and Middelgrunden, in Sweden at Lillgrund, in Germany at Baltic, in Britain at Barrow, North Hoyle, Kentish Flats, Scroby Sands, Thanet, and Robin Rigg, and in the Netherlands at OWEZ [3]. In addition to maintenance penalties, mechanical damage to the wind blades reduces the electrical efficiency of the wind turbines. Wind tunnel experiments estimate a 5%

reduction of the total energy capture, depending of factors such as the type and degree of surface roughness of the blade [3].

Wind turbine blades are primarily made of fiberglass reinforced polymer composites. Skins are typically double-bias or triaxial fiberglass and the core is made of balsa or some kind of foam structure. Epoxy-based materials have been the preferred choice of binder due to their high strength, easy production and low cost. Carbon fibres are often used for local reinforcement. Compared to epoxy-based materials, carbon fibres have higher modulus, lower density, higher tensile strength and lower fatigue sensitivity [4].

Although there is no precise data available, a substantial fraction of the new large-blade wind turbine installations uses blade coating systems. These coating systems have the ability to absorb the energy from impacting droplets and are expected to provide efficient and long term, cost-effective protection against rain erosion. However, commercial blade coating technology is relatively recent and performance data for long term exposure (>15 years) are not available.

Current blade coating systems consist, typically, of a putty layer which is applied for filling pores in the composite substrate, a primer to secure good adhesion of the subsequent coat and a flexible topcoat, usually a polyurethane-based formulation [5].

The preferred method for evaluating rain erosion has been the so-called "whirling arm" test, developed by the Radiation Laboratory at MIT in 1946 [6]. Fundamentally, the whirling arm consists of a rotor, 2 m in diameter, rotating in an imposed artificial rainfall. Erosion data obtained in the whirling arm setup for polyurethane and neoprene aircraft coatings correlated very well with actual flight tests [7, 8]. In recent years, the whirling arm rig has been used for testing coating systems for wind turbine blades. The tip speed of wind turbine blades can presently get up to 100 m/s, about one third the speed of commercial passenger flights and about one fifth the speed of fighter jets. Whirling arm tests last for a few hours with a tip speed of 150 m/s and in most cases three samples, one on each rotor blade, are used simultaneously. It is not clear that in the case of wind blades the accelerated whirling arm test will provide representative data (3 hours of accelerated "heavy rainfall" versus up to 20 years natural exposure), but in absence of alternatives the whirling arm test has become an acknowledged test method for the approval of coating systems for wind blades. However, we understand that coating companies do not have whirling arm equipment

available in-house and therefore must rely on external laboratories for the testing of their coating systems.

The purpose of this work is to design, construct and run a simple laboratory setup based on the water jet principle. The proposed setup may be used for the initial screening experiments of blade coating systems prior to the final approval in the whirling arm rig. The setup must involve low capital and operational costs, have a low footprint, are able to run many samples simultaneously and, most importantly, must be able to produce data that correlates satisfactorily with the experimental data obtained with the whirling arm test. Various modifications of the original prototype have been evaluated in an attempt to produce such a good correlation.

2.3 Previous experimental setups simulating liquid impact erosion

There have been many previous attempts to simulate liquid erosion in the laboratory. In this paragraph, a concise overview of the various types of equipment is presented to provide background knowledge. More detailed and chronological descriptions are available in previous review articles (from 2002 or older) [2, 9-13]

A variety of test rigs have been proposed. The basic difference among these rigs is the active/passive impact mode between water droplets/jets and test specimens. Each facility has its own advantages and drawbacks and the selection of the specific type of equipment is based on the pertinent application and specific requirements for efficiency and cost. Table 2.1presents a comparison of the various available setups.

Table 2.1 Historical overview of liquid erosion experiments.

Type of water erosion	Rig names	Relevant parameters	Advantages	Drawbacks	First time reported
Impacting continuous water jets	Wheel and jet [14-16]	Jet diameter 0.3 – 2.5 mm. Maximum impact velocity 600 m/s.	Simple fabrication and operation.	Poor reproducibility.	1924
	WJA (conventional water jet erosion apparatus) [44]	Impact velocity 0-40 m/s. Impact angle 90°.			1997
Water jet provoked impacting droplets	Not available [18-22]	Impact velocity 0-350 m/s. Impact angle 90°. Droplet size <1 mm.	Cheap to fabricate and operate. Good test results for some materials.	Low reproducibility. Low test efficiency. Uncontrollable ambient conditions.	2007
Impacting water jet slugs	MIJA (multiple impact jet apparatus) [6, 23, 26, 30, 36, 38]	Impact velocity 30-600 m/s. Nozzle orifice to specimen 10 mm. 20 impacts per minute.	Inexpensive rig. Well controlled testing parameters. Reproducible results. Reproducible jet profile. Narrow velocity spread (0.5-1.5%). Flexible sample size, shape and material.	High experimental skills required. Only jets can be generated.	1991
	Discrete jet (or interrupted jet) [1, 6, 31, 32]	Not available	Cheap to fabricate and operate. Useful for a limitted range of materials.	Inaccurate results.	1957
Moving samples impacting falling water droplets	Whirling arm [7-9, 27, 33-38]	Characteristic droplet size 2 mm. Rainfall 25.4 mm/h. Impact angle 0-60°. Impact velocity 0-300 m/s.	Reproducible results. Results correlate well with practical flight testing. Good for comparison of relative erosion resistance.	Expensive fabrication and operation. Complex aerodynamic environment. Assumed predetermined impact environment changes as velocity changes. Actual drop size different with prdetermined size. Not precise for erosion mechanism study. Poor interchangeability of test results among rigs of same type. Low test efficiency.	1946
	GRCl Ballistic range [6, 23, 36, 38]	Droplet size 1.5-5.0 mm. Impact angle 0-60°. Impact velocity 100-1000 m/s. Maximum cylinder diameter 20 mm.	Both spherical and distorted water drops can be generated. Both single and multiple impacts modes available. Excellent reproducibility. High velocity available. Consistent correlations between impact velocity, droplet size and impact angle. Direct correlation between cause and effect. Excellent for erosion mechanism study.	Expensive fabrication. Low test efficiency. Only small samples possible. High experimental skills.	1976
	Wind tunnel [6]	Artificial rainfall 0.3 l/s. Water concentration 50-100 times higher than real environment. Impact velocity 200-275 m/s. Useful test time 100 s. Specimen diameter 260 mm.	Results correlate well with practical flight testing.	Expensive fabrication. Low test velocity. Short useful testing time. Unrealistic droplet concentration. Temperature difficult to control. Droplet size hard to control. Results difficult to compare with other rigs.	1965
	Holloman Rocket sled [6, 36, 38]	Rainfield 1800 m. Maximum velocity 2000 m/s. Impact angle 0-70°.	Consistent data. Results correlate with practical flight testing. Extremely high impact velocity possible. Small to full-scale objects can be exposed.	Extremely expensive to fabricate and test. Samples suffering from shock wave effect. Different water drop concentration distribution. Low test efficiency.	1957

2.3.1 Impacting continuous water jets

The first experimental investigation of liquid erosion by repeated impact is the so-called "wheel-and-jet", which has been used in various forms since the 1920s. The principle is to attach specimens on the periphery of a rotating disk or arm and let the specimens pass through one or more continuous liquid jets [6, 14-16]. This method has been used for liquid erosion of alloys. A modified version keeps the sample material at rest and let a continuous liquid jet deliver the impact [16]. The jet is produced by a high pressure pump. The continuous jet was useful for studying erosion mechanisms and provided a ranking of selected materials, such as alloys and brittle polymeric coatings (PMMA). Careful calibration and correlation experiments are needed to ensure meaningful results.

2.3.2 Water jet provoked impacting droplets

A liquid jet leaving a nozzle into an ambient atmosphere is unstable and will, at some distance, break into droplets of sizes comparable with the jet diameter or much smaller [17]. Some researchers, in recent years, used this method to investigate erosion mechanisms and compare material (e.g. alloys and polymeric coatings) performances [18-22]. The distance between nozzle and specimen is critical for proper droplet formation. However, droplet sizes have been characterized by doppler anemometry and found to be much less than a typical rain droplet diameter of 2 mm [23].

2.3.3 Impacting water jet slugs

Theoretical and experimental studies have indicated that short liquid jets (so-called jet slugs) can be used to simulate droplet impact [11, 24]. The reason is that the central core of a short coherent liquid jet has a smooth, slightly curved, front profile, which allows a reasonable representation of a water droplet. Bowden and Brunton [25] devised such a rig, SIJA (single impact jet apparatus), where sample materials were kept at rest and short jets of liquid were used for impact. Materials investigated were hard polymers for aircrafts. Results showed that evaluation of high velocity erosion by this rig can be achieved. An advanced water jet impact rig named MIJA (multiple impact jet apparatus) with computer control and multiple impacts was devised and tested between 1982 and 1991 [26-29]. It produced a jet every 5 s with velocities ranging from 30 to 600 m/s. The jet slug is formed by extruding liquid through an

orifice [30]. The damage produced can be correlated very well with that occuring during an actual flight at high velocity through a rainfall [28].

Another way to generate jet slugs is by the use of a discrete jet (or interrupted jet) apparatus. The first description of such a rig was provided by Olive in 1953 [1]. In this setup, a high pressure pump forces a continuous jet of water, at a selected velocity, through nozzles with specific diameters, thereby generating a specific jet cylinder radius. A slotted rotating stainless steel disk chops the jet into discrete slugs. Photographic characterization showed that the jets are cigar-shaped [1]. Recently, this principle was used for water erosion evaluation of alloys [31]. It is claimed that this technique can provide valuable data on the relative erosion resistance of different alloy samples and that a good correlation exists with whirling arm test results [31, 32].

2.3.4 Moving samples impacting falling water droplets

The principle of this type of equipment is to simulate the impact taking place when a moving object is exposed to a rainfall. The most well-known rig is probably the whirling arm equipment, which has been used extensively for rain erosion experiments since the 1940s. The erosion is achieved by rotating three arms ("rotors") at high velocity in an artificial rainfall, formed by spraying water through nozzles [33]. Average droplet diameters of 2 mm appear to have been adopted by most investigators as the "standard" droplet size and 25.4 mm/hour (1 inch/hour) as the standard rainfall rate [8]. A series of real flight tests in rain have shown that whirling arm test results could be correlated well with the actual flight test results without negative effects from the high centrifugal force of the whirling arm [7]. Experiments showed not only the same ranking, but also the same failure mode for the materials investigated [6]. According to several authors [2, 6-9, 27, 34-37], the whirling arm facility is a very useful tool for evaluating the erosion-resistance of materials (e.g. screening tests). A simple equation for the whirling arm rig, providing a relationship between impact frequency, f_w (impacts/m^{2}s), impact velocity, v_w, and liquid volume fraction of the experimental chamber, φ_w, can be derived

$$f_w = \frac{v_w \varphi_w}{\left(\dfrac{\pi}{6} d_p^{\ 3}\right)} = \frac{v_w \left(\dfrac{l_o}{t_T v_s}\right)}{\left(\dfrac{\pi}{6} d_p^{\ 3}\right)}$$

(1)

where the ratio, l_o/t_T, is the rainfall rate and v_s is the steady state water droplet sedimentation velocity in the air chamber. For a droplet diameter of 2 mm (equivalent to a sedimentation velocity of about 7 m/s according to "Newton's sedimentation law"), a rainfall rate of 25.4 mm/h, and an impact velocity of 150 m/s, the water droplet impact frequency can be calculated to 36101 impacts/(m^2·s).

To achieve a well-controlled impact environment, another rig has been constructed, where a material sample is attached in the front of a so-called sabot (i.e. "like a bullet"), which can be propelled down a tube using a small charge of gunpowder. The material sample then impacts a falling water droplet, which has a well-controlled size and shape. The complex process requires high experimental skills [6, 9, 38]. This method is a further development of the old suspended water droplet principle, which can cause distortion of the water droplet. Another variation of this equipment involves a gun barrel, a rain section and a breaking section, and the specimen is launched by gun powder or a compressed air blast. These ballistic range techniques can achieve the velocity with a controlled temperature and pressure which produce well controlled parameters for mechanistic studies of water erosion. The drawbacks are the time and expense per shot and the restriction in the sample size. Useful information on water droplet erosion has also obtained by this technique [6].

The erosion test facilities "rock sled" and the wind tunnel are based on a similar principle by propelling the material sample through an artificial rain field. Disregarding its huge size, these techniques allow the use of very high velocities and aerodynamically appropriate geometries [6]. However, due to the huge costs of construction and operation of the facility, those techniques are restricted to very few research centers.

2.4 Design criteria for water jet setup

We have not found any previous studies of water droplet erosion of blade coatings in laboratory setups. It was decided to base the new setup on continuous water jets and impacting water jet slugs. In an attempt to obtain some kind of correlation between the whirling arm rig and the new water jet setup, design criteria need to be chosen. However, there is a fundamental difference between a coated panel moving in a heavy rainfall, as in the whirling arm rig, and a continuous or discontinuous water jet impacting a slowly moving coated panel. For a setup similar to the whirling arm rig, it has been shown, using a high-speed camera [39], how a water drop of average size 2

mm is shattered into thousands of smaller drops upon impact with a coated panel moving at high velocities. A similar, but not identical, event takes place when a discontinuous water jet impacts a coated panel and it is an assumption of this work that the mechanisms are sufficiently similar to allow a correlation between the two setups. The assumption will be discussed in more detail in the results and discussion section.

The impact of liquid will generate several different pressure waves in the coating that can cause material damages [25, 40]. It has been chosen to scale the two rigs based on the water hammer pressure and the impact frequency. The water hammer pressure is given by the equation

$$P = \rho C v \tag{2}$$

where ρ and C are the density and acoustic velocity of the water, respectively, and v is the impact velocity. To match the water hammer pressure in the two rigs, the rotor tip and jet velocity simply need to be identical. The droplet or jet impact frequency [measured in the unit impacts/(m^2·s)] is also essential because of the importance of relaxation times in coatings. The ability and rate of a coating to absorb and distribute the energy from an impact (resiliency) can vary tremendously and this difference will be expressed via the impact frequency. The latter can be approximately matched by a proper choice of process parameters in the jet setup as will be shown later. There are also differences between the two rigs, which are expected to cause secondary effects. The most important ones are probably the geometry or curvature of the coated panels and the potential presence of a thin water film on the coating, formed by the previous impacting droplet or jet slug. In the whirling arm rig, the panels have a curved shape, similar to wind turbine blades, and the fast movement of the rotor may rapidly remove any water film, whereas an imposed "wind" will need to be arranged in the jet setup to realize a similar situation. Finally, droplet geometry and size, impact angle, and water temperature may also be of importance. The new setup should be able to run many samples simultaneously.

2.5 Experimental procedures

2.5.1 Design and construction of water jet erosion rig

Initially, a setup based on a continuous flat fan jet, was constructed. A schematic illustration of the equipment line is shown in Figure 2.1.
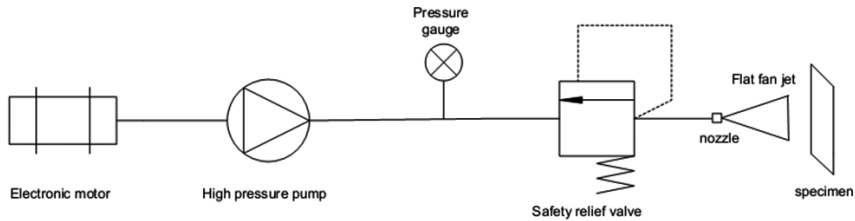
Figure 2.1 Rig V1- Schematic illustration of the continuous flat fan water jet erosion rig. Water for the jet is taken from a tank (not shown in figure) holding about 50 liters of water (no recycle was used).

The rig utilizes a high pressure plunger pump, UDOR MSC 16/20 S, to produce the jet. The fan size formed is dependent on the nozzle fan angle. The PNR1686 nozzle with 25º fan angle and 1.12 mm equivalent orifice diameter was used for the flat fan jets. The safety relief valve was installed to avoid building up too high pressures. Tap water was used as the eroding liquid for all the experiments. The average linear water jet velocity (in m/s) at the orifice of the nozzle can be calculated from the volumetric water flow rate (in m^3/s) divided by the cross section area (in m^2) of the nozzle. The instantaneous pressure readout was monitored by a pressure gauge. The distance of nozzle orifice to sample surface was kept at 10 cm so that the decrease of jet velocity, due to air friction within this short distance, could be neglected. The high pressure water jet will cause a water temperature increase, but this was avoided by using either a once-through principle for the water or a thermostated water bath.

To obtain a more realistic physical situation than the continuous jet, a modification of parts of the setup was conducted. The Lechler 546 nozzle with 0.84 mm orifice diameter was used for the continuous straight jets. A close-up of this part is shown in Figure 2.2.
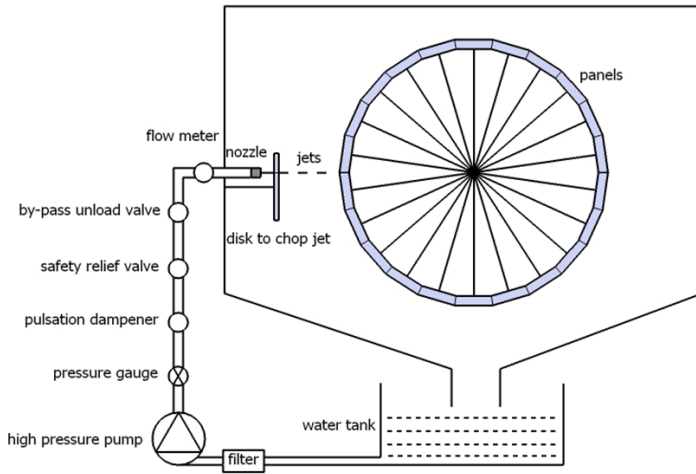
Figure 2.2 Rig V2 – Schematic illustration (vertical cross-sectional view) of water jet erosion rig, including the disk, which ensures discrete water jets. The water recirculation tank holds about 50 liters of water.

The moving wheel (diameter of 52 cm) in the middle of the chamber, holding up to 22 coated steel panels, is driven by an electronic motor (power input of 0.25 kW), allowing for various rotation velocities (0.1-4.5 RPM). The water flow rate can be varied by regulating a by-pass unload valve, whereby the water jet velocity at the nozzle orifice can be controlled. The pulsation dampener ensures a stable jet. A digital flow meter was installed to measure the water flow rate. A rotating stainless steel disk (diameter of 10 cm), with 10 mm holes as shown in Figure 2.3(1) or with 1 mm slots as shown in Figure 2.3(2), was incorporated into the rig to chop the continuous straight water jet into slugs; the modification is shown in Figure 2.3(3). This addition enabled an investigation of effect of droplet impact frequency and size of jet slugs. The moving wheel holding the coated panels is shown in Figure 2.3(4).
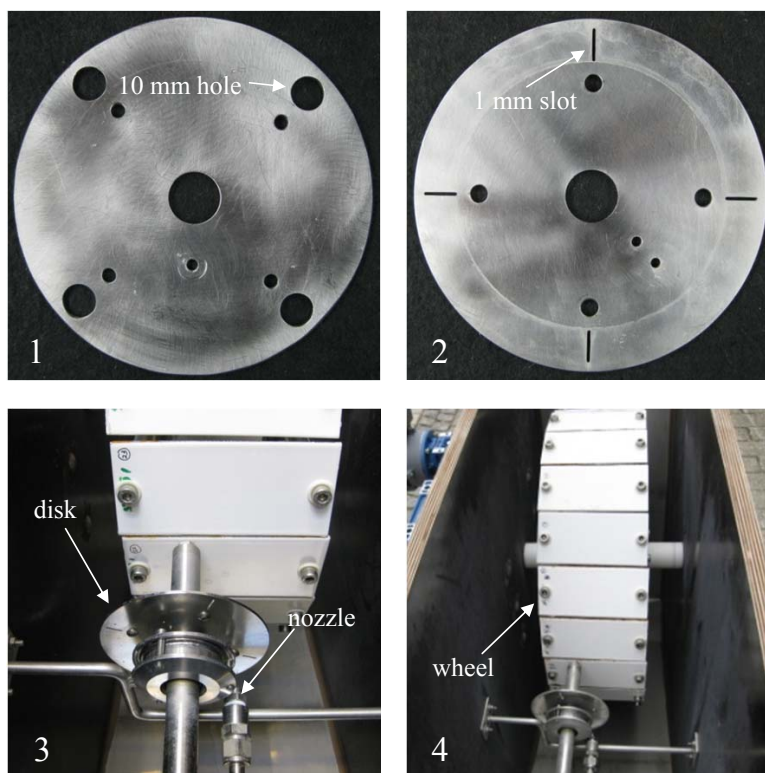
Figure 2.3 Disks with (1) 10 mm diameter holes and (2) 1 mm slots for chopping water jets. The smaller holes seen in the disk are used for fixation of the disk in the jet setup. Insert (3) shows the disk position in the rig and insert (4) the wheel with 22 coated panels.

2.5.2 Details of coated steel panels

Flat steel panels of dimensions 7.0×15.0 cm and a thickness of 2 mm were used as substrate. The latter was firstly coated by an epoxy primer followed by two different polyurethane-based blade coatings (topcoats), termed coatings A and B. Both coatings contain xylene and polar solvents (butyl acetate type). The binder of coating A consists of a common commercial polyester polyol cured with a common commercial flexibilized isocyanate trimer. For Coating B, the same polyester polyol as for coating A was used and the curing agent was a standard isocyanate trimer. Both coatings contain colouring pigments (mainly TiO_2) and standard extenders. Coating application was done using airless spray at 200 bars and cured at 23 °C for 7 days, following one hole drilled on each end of the panel to attach them to the moving wheel. The total dry film thickness (DFT) of primer and topcoats, measured using an Elcometer Model 355

Top, calibrated for 450 µm thickness, was 423.3±51 µm for the coating A system based on 30 separate samples and 421.6±91 µm for the coating B system (also 30 separate samples).

2.5.3 Comparative experimentation in whirling arm rig

For the purpose of comparison, the two coating systems were also tested externally in a whirling arm rig at a controlled temperature of 20-25 °C. The rotor blade radius was 0.915 m and the rainfall intensity 30-35 mm/hour. The water droplet size was 1-2 mm and the tangential velocity of the coated steel panel, due to the radial dependency, ranged from 126 to 160 m/s. The coated steel panel, with a curved geometry that simulated a rotor blade leading edge, is shown in Figure 2.4.

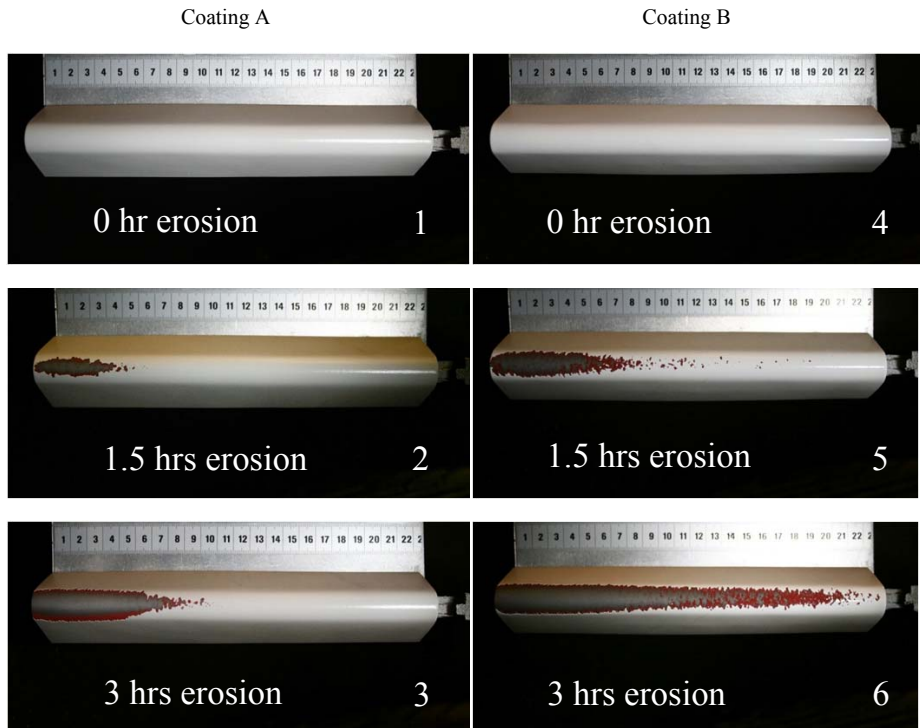Figure 2.4 Results of rain erosion experiments in a whirling arm rig with two blade coatings. The highest impact velocity (rotor tip) was to the left on the panels, where erosion damage is most visible. The three left hand photos show Coating A before (1) and after erosion (2-3). To the right, Coating B, before (4) and after erosion (5-6), is seen. The scale shown in the figures is in cm.

The special curvature of the panels was established prior to coating application. For efficient use of the rather expensive curved steel substrates, coatings were removed by sand blasting after experimentation and reused. The length of a test panel is 22.5 cm. Erosion was evaluated by inspecting samples every half an hour with all total test duration of 3 hours.

2.5.4 Characterization methods

Incubation time, defined here as the time period prior to erosion damage appearing, is critical for blade coatings. Surface defects may result in a loss of aerodynamic balance of the wind turbine and the coating erosion rate is likely to accelerate after a damage appear [41, 42]. Therefore, attention was paid to incubation time and this output parameter was recorded during each experimental series.

During our initial experiments, where an even flat fan jet and wheel rotation were used, weight loss measurements were recorded at regular intervals. Coating samples were removed from the rig at predetermined time intervals, gently washed with fresh tap water to remove any loose coating remains and finally gently wiped to remove any residual water. Then samples were dried in a forced-convection oven at 50 ºC for 1 hour, until a constant sample weight was obtained. Using this method, it was actually possible to quantify the erosion rate, but when using a straight jet (and a rotating wheel), the area eroded was too small for an accurate detection and the approach was abandoned.

Once erosion occurs, morphology change will appear. This change can be detected on a photo of the damaged coating using the software ImageJ, whereby the eroded area can be calculated. This characterization method was investigated in one of the experimental series. In addition, the morphology of coating surface was characterized with and without erosion by Alicona infinite focus optical surface metrology.

The adhesion (pull-off strength) of the coating system was investigated by gluing a so-called "dolly" (metal object with a flat base) onto the coating surface, using epoxy glue, followed by a machine-driven pull-off removal of the dolly, while recording the force required. This technique is known as pull-off adhesion test method.

2.5.5 Experimental erosion procedure

Using rig V1 (see figure 2.1), the two wind turbine blade coatings were exposed to jet erosion at stationary conditions. Experiments were initiated by filling the hold up tank

with water, turning on the wheel and/or the disk to the selected rotation velocities, and finally the high pressure pumps, driving the water jet, were started and adjusted to the required pressure (jet velocity). The jet is focused on a small area on the coating surface. During experimentation in rig V2 (see figure 2.2), where the coating sample is continuously being moved in front of the jet by the wheel, the coating area exposed to the flat fan jet (in one pass) is approximately 4.4 × 7.0 cm, when the distance between the coating surface and the nozzle orifice is 10 cm. The coating exposed to the straight jet (and wheel rotation) is only damaged in a small area of about 2 mm × 7 cm, however, this area was more than enough to detect erosion damage and the non-exposed coating area may be exploited for additional experiments in a more flexible equipment. The experiment was periodically put to a halt to examine potential coating failures, such as cracking, fracture, cratering, pitting, penetration to the substrate, adhesion loss between coatings or delamination at the coating substrate interphase. Photos of the coating surfaces were regularly recorded.

2.5.6 Mathematical model linking process parameters in water jet setup

As described in an earlier section, it is important to approximately match the water hammer pressure and the impact frequency in the two rigs. This is only possible when the rotating disk is employed (i.e. for a non-continuous jet). A mathematical model is required to link the different parameters in the water jet setup. The impact frequency of a discrete water jet, f_j (impacts/m²s), can be expressed as

$$f_j = \frac{1}{t_B A} \tag{3}$$

where t_B is the time between two impacts and A is the exposed coating area during this time interval. From the definition of velocity one gets

$$t_B = \frac{l_B}{v_D} = \frac{l_B}{2\pi f_D R_D} \tag{4}$$

where l_B is the distance between two holes on the disk and f_D and R_D is the frequency and radius of the disk, respectively. The exposed coating area A is given by

$$A = \frac{\pi}{4} d_h{}^2 + d_h l_{wh} \tag{5}$$

with

$$l_{wh} = t_B v_{wh} = t_B 2\pi f_{wh} R_{wh} \tag{6}$$

where l_{wh} is the distance moved by a coating panel during time t_B. If the wheel is not moving then l_{wh}=0. If the impact frequency of the whirling arm rig is termed f_w then the ratio of the two impact frequencies will be

$$\frac{f_j}{f_w} = \frac{2\pi f_D R_D}{l_B f_w \left[\frac{\pi}{4} d_h^2 + \frac{d_h l_B f_{wh} R_{wh}}{f_D R_D} \right]} \tag{7}$$

where f_w can be calculated from equation (1) (an example is provided in section 2.3.4). The impact frequencies of the two setups will be matched when f_j=f_w (or f_j/f_w=1) and the following parameters in the jet setup can be adjusted to realize that: f_D, R_D, l_B, d_h, f_{wh} and R_{wh}. Practical considerations in the design of the setup have put constraints on R_{wh}, l_B, d_h, and R_{wh}, f_D and f_{wh} are left as free parameters that can be used to adjust the conditions to f_j/f_w=1.

2.6 Results and discussion

A series of experiments was conducted using the new water jet setup. Two blade coatings, termed A and B, were selected for the development of the experimental setup. In Figure 2.5, a schematic flow chart of the experimentation strategy (as it developed) is shown.
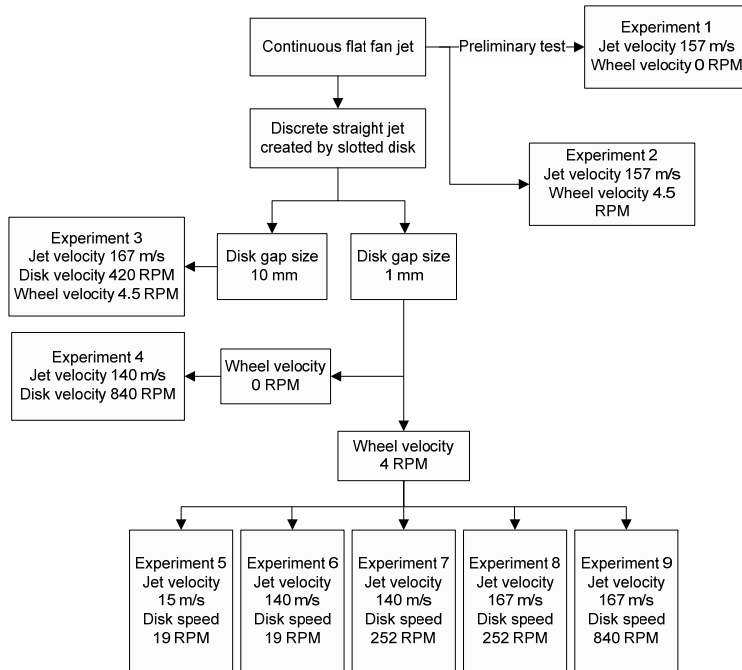
Figure 2.5 Overview of experiments conducted in the water jet setup. The chronological order of the experiments was from Experiment 1 - Experiment 9.

First, we conducted initial trials with a continuous jet, a flat fan nozzle, and a static wheel (Experiment 1). The proposed setup was then modified including a moving wheel and employing 22 panels simultaneously (Experiment 2). Secondly, the advanced rig with a slotted (10 mm) disk and a circular nozzle was used for experimentation with discrete jet slugs (Experiment 3). The remaining experiments were done using a smaller disk gap size (1 mm), first with a static (Experiment 4) and then with a moving wheel (Experiment 5-9). In Experiments 5-9, the influence of the jet velocity and the disk rotation frequency were investigated. All water jet results are summarized in the Table 2.2.

Table 2.2 Overview of process parameters and results for experiments in water jet erosion rig. The result "Coating B > Coating A" means that the performance of coating B was better than that of coating A.

Experiment No.	Nozzle Diameter (mm)	Jet type	Jet velocity v_j (m/s)	Disk gap size (mm) d_h	Disk rotation (rpm) f_D	Wheel rotation (rpm) f_{wh}	Ratio of impact frequencies f_j/f_w	Experimentation time (hrs)	Damage description	Result (ranking)
1	1.12	Continuous flat fan jet	157 (200 bar)	N/A	No disk	0	∞	1/6	Coating A started pitting in 30 secs Coating B started pitting in 10 mins	Coating B > Coating A
2	1.12	Continuous flat fan jet	157 (200 bar)	N/A	No disk	4.5	∞	4	Coating A started pitting in 2/3 hrs Coating B no damage in 4 hrs	Coating B > Coating A
3	0.84	Discrete straight jet	167 (150 bar)	10	420	4.5	14.0	3	Coating A started pitting in 1/3 hrs Coating B no damage in 3 hrs	Coating B > Coating A
4	0.84	Discrete straight jet	140 (100 bar)	1.0	840	0	4200.0	8	Coating A damaged in 3 hrs Coating B no damage in 8 hrs	Coating B > Coating A
5	0.84	Discrete straight jet	15 (20 bar)	1.0	19	4	1.0	66	No erosion for both samples	N/A
6	0.84	Discrete straight jet	140 (100 bar)	1.0	19	4	1.0	66	No erosion for both samples	N/A
7	0.84	Discrete straight jet	140 (100 bar)	1.0	252	4	157.0	66	No erosion for both samples	N/A
8	0.84	Discrete straight jet	167 (150 bar)	1.0	252	4	157.0	66	Coating A started pitting in 60 hrs Coating B no damage in 66 hrs	Coating B > Coating A
9	0.84	Discrete straight jet	167 (150 bar)	1.0	840	4	1349.0	66	Coating A started pitting in 25 hrs Coating B no damage in 66 hrs	Coating B > Coating A

In the whirling arm rig, coating A showed higher erosion-resistance than coating B (approximately the same for three replicates of each coating) as shown in Figure 2.4. After 1.5 h, the length of the damaged areas in sample A and B were approximately 5 and 19 cm, respectively. After 3 hours of experimentation, the length of the damaged area for the coatings A and B were about 10 cm and the entire coated panel 22.5 cm, respectively.

The erosion damages of the coatings take place in 3 hours in the whirling arm experiments (samples continuously exposed). Therefore, with 22 panels fitting in the new setup (continuous operation, but samples exposed sequentially on the wheel), the erosion should take place in not more than 66 hours for the panel exposure time to be identical in the two setups. Data from the water jet setup will now be discussed in more detail.

2.6.1 Erosion of coatings by continuous flat fan jet

The preliminary experiment (Experiment 1) with a continuous flat fan water jet was done in rig V1 (Figure 2.1) using the parameter values shown in Table 2.2. Erosion was very rapid; for coating A it started after only 30 s and for coating B it started after about 10 minutes. The failure of the two coatings is shown in Figure 2.6.
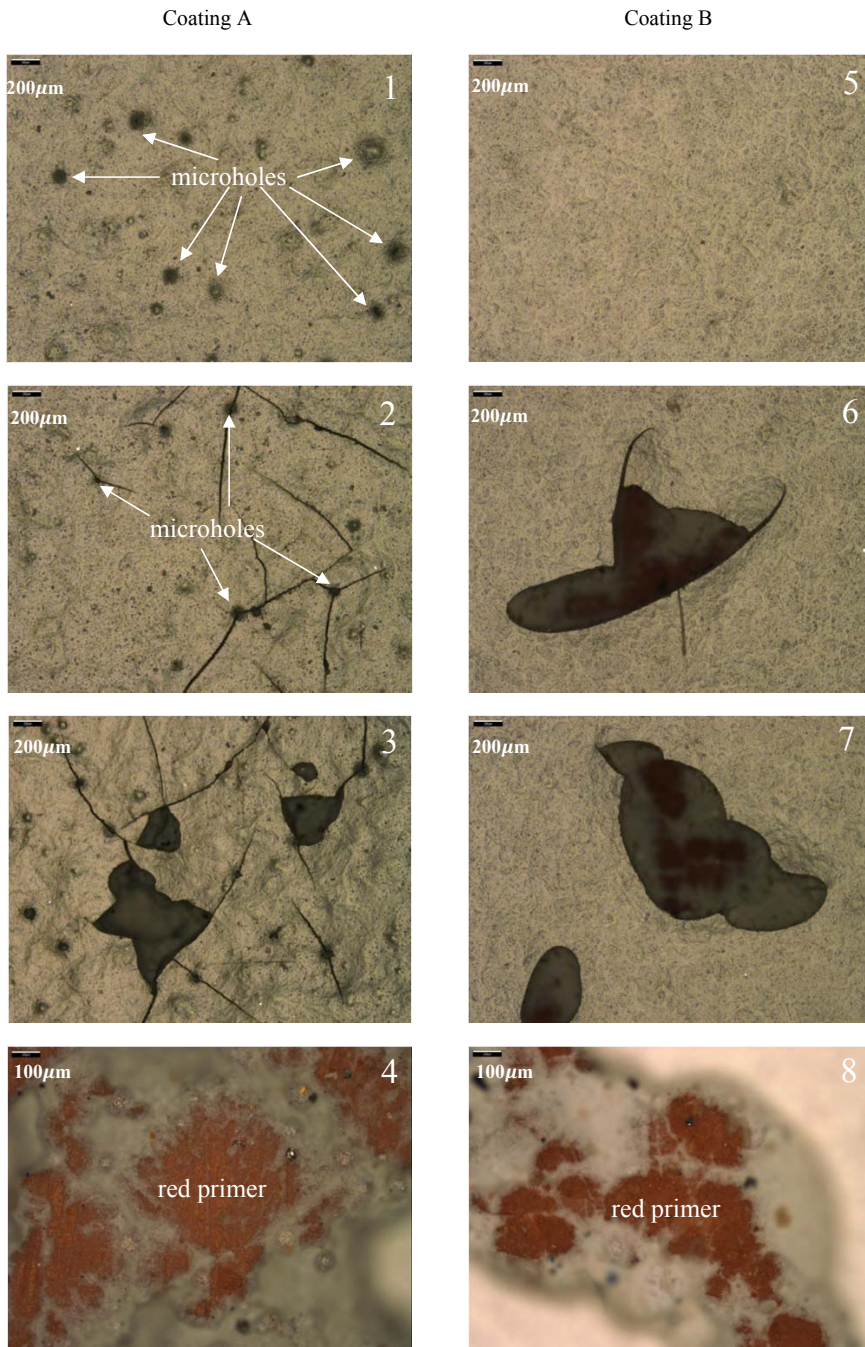
Figure 2.6 Microscopic photos of coating A after 30 seconds exposure and coating B after 10 minutes exposure using a continuous water jet. To the left, Coating A before (1) and after erosion (2-4) is shown. To the right, Coating B before (5) and after erosion (6-8) is seen.

Prior to exposure, Coating A had microholes in the surface, but otherwise showed no sign of defects. Following the experiment the sample showed delamination and cracking and the underlying primer was visible. Cracking appear to run through or to initiate from the microholes. Coating B no defects were visible prior to exposure, but it was partly delaminated after the failure mechanism had set in and cracks were also visible, although to a lesser extent than for coating A. The underlying red primer was also visible after exposure in this case. Even though both coatings failed, coating B lasted about 20 times longer than coating A. This result is in contradiction with that obtained in the whirling arm, where the ranking was opposite.

The next experiment, Experiment 2, was conducted in the rig V2 (Figure 2.2) which incorporated a rotating wheel. The average velocity of the flat fan jet was about 157 m/s and three replicates of each coating was used so that the repetability of the experiments could be investigated. Figure 2.7 shows the average eroded surface area of the three samples of each coating system, measured using image analysis.
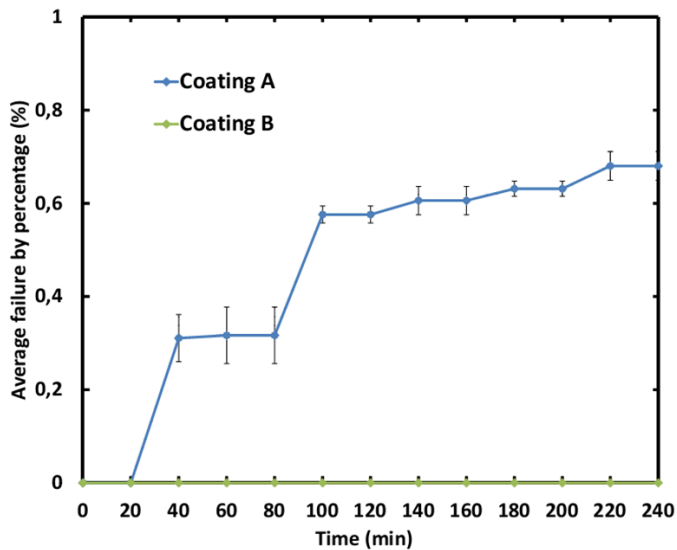
Figure 2.7 Experimental data of fraction of exposed coating area eroded in water jet setup. Standard deviations are shown as error bars. Coating B coincides with the x-axis.

Note that in all cases, less than 1 % of the coating surface area exposed was visually damaged. The incubation period of coating A, during which the erosion of the specimen cannot be measured, was found to be between 20 and 40 minutes only, whereas for coating B there was no erosion visible even after 6 hours. Coating B

exhibited excellent water jet erosion resistance. In Figure 2.8, the average weight loss versus experimentation time for coating A and B is shown as a supplementary evaluation method.
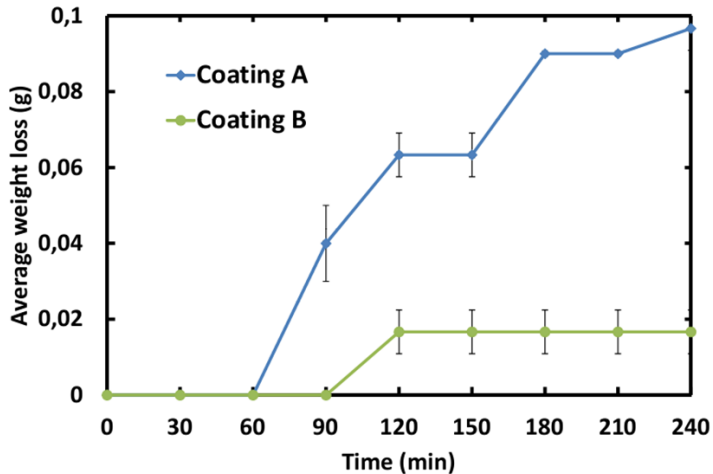
Figure 2.8 Experimental data of weight losses from coatings as a function of experimentation time. Standard deviations are shown as error bars.

The weight loss changes gradually with time and is repeatable. For this method, Coating B also showed superior erosion performance over Coating A. In fact, the weight loss was so low that it was almost comparable to the accuracy of the weighing scale. In this case, the erosion resistance ranking for the two investigated coatings is also opposite to the ranking of the coatings in the whirling arm rig.

2.6.2 Erosion of coatings by discrete straight jet

Experiment 3 and 4 were done in the V2 setup with variations in the disk gap size, disk velocity, jet velocity and wheel velocity (parameter values employed are shown in Table 2.2 and Figure 2.5). The results were similar in these two experiments with no erosion observed in coating B and fast (20 min) to fairly fast (3 hours) erosion of coating A.

2.6.2.1 Effect of water jet velocity

In Experiment 5, parameters were set so as to "equalize" the impact frequency of the two setups (water jet and whirling arm), while keeping a low water jet velocity. In this case, however, there was no erosion after 66 hours on both coatings. Then the impact

velocity was increased to 140 m/s (Experiment 6) and the disk frequency was increased to 252 RPM (Experiment 7) with other parameters remaining constant. Also in those two cases there was no erosion of any of the coatings. The impact velocity was then increased to 167 m/s (Experiment 8) and erosion of coating A was found after 60 hours (visual evidence is shown in Figure 2.9) while Coating B did not show erosion. This indicates that there is a critical jet velocity for the initiation of erosion at least for Coating A. Below this velocity; the coatings did not show erosion even after prolonged exposure. Impact velocity, in good agreement with equation (1), appears to be the most critical element governing the initiation of erosion.
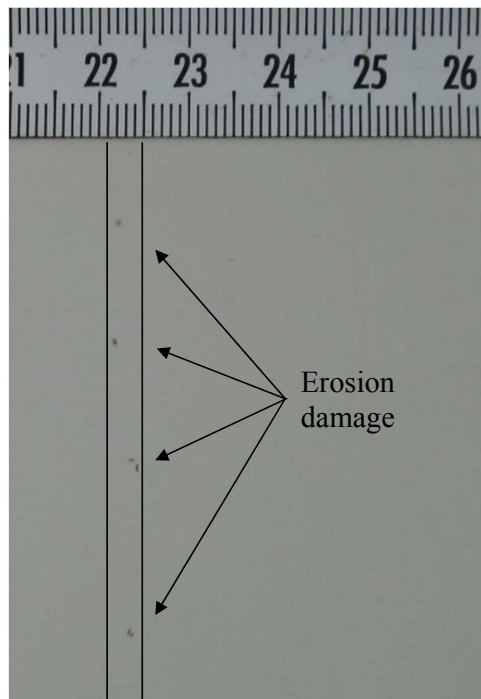
Figure 2.9 Photo of Coating A showing erosion damage after 60 hours. The scale is in centimeter. The area between the two solid lines was exposed to the water jet slugs.

2.6.2.2 Effect of impact frequency

Elastic coatings for blades have unique properties compared with rigid polymeric materials. Their ability to recover mechanically between impacts gives them their superior erosion resistance. If the time between successive droplet impacts is shorter

than the relaxation time, it will cause cumulative strain in the coating, which eventually leads to failure. Therefore, impact frequency is expected to be an important parameter. However, the results of Experiment 6 and 7, where the impact frequency varied by a factor of 157 (f_j/f_w=1 in experiment 6), showed no erosion of the two coatings.

When the disk frequency increased from 252 RPM (Experiment 8) to 840 RPM (Experiment 9), corresponding to an additional factor of 8.6 on the impact frequency, the time to initiation of erosion decreased from 60 to 25 hours for coating A (no erosion for coating B). Thus, impact frequency does matter, but in a more complex way than anticipated. However, if the jet velocity is not high enough for erosion initiation, then an increase of impact frequency did not influence coating erosion or damage even after long exposure time.

2.6.2.3 Measurements of adhesion strength

To analyse for less visible defects, pull off adhesion evaluation experiments were conducted on the non-exposed coatings. Photos of the visual adhesion losses observed are shown in Figure 2.10 and analysis results are provided in Table 2.3.

Figure 2.10 Photos showing results of pull-off adhesion experiments on non-exposed coatings. The bases of the detached dollies are shown to the right in each photo.

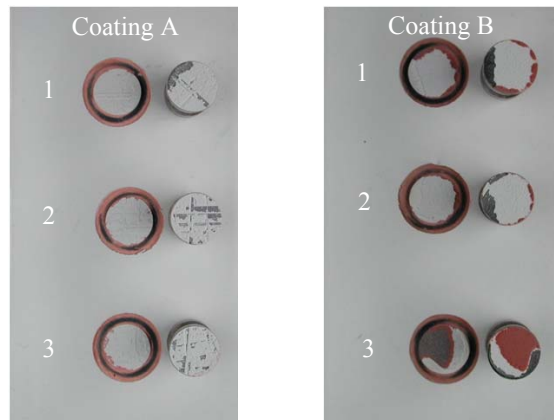Table 2.3 Results of pull-off adhesion analysis. The values reported represent the percent failure of the area covered by the dolly base.

	Coating A (failure by percent of area)			Coating B (failure by percent of area)		
	Dolly 1	Dolly 2	Dolly 3	Dolly 1	Dolly 2	Dolly 3
Cohesive failure of topcoat	90	90	90	80	80	10
Adhesive failure between topcoat and glue	10	10	10	15	15	10
Cohesive failure of primer	0	0	0	5	5	0
Adhesive failure between primer and substrate	0	0	0	0	0	80

No adhesive failure between topcoat and primer was observed for the non-exposed coatings. However, for exposed panels, delamination between topcoat and primer was observed for both blade coatings as shown in Figure 2.6(4) and 2.6(8). Therefore, the delamination between topcoat and primer was caused by repeated water jet impacts.

2.6.2.4 Mechanistic discussion of coating degradation

Prior to water jet exposure, blade coating A had various "conventional defects" (microholes) as shown under microscope in Figure 2.6(1). These defects may originate from the application procedure, incompatibility of coating ingredients, or some kind of surface contamination (e.g. dust particles with a low surface energy). After water jet exposure, small cracks are seen to connect some of the microholes in the coating [Figure 2.6(2)]. Therefore, the microholes are potentially weak points and may act as sites for crack initiation when the samples are exposed to droplet impacts. It may be noted that a similar degradation mechanism has been observed for cavitation erosion of coatings [2]. The initial cracks are likely to propagate and at some point cause a visual failure. The growth of cracks in the polyurethane coating, shown in Figure 2.6(3), may occur through progressive chipping of material from the border of the delaminated area. Lateral jets impacting the periphery of the pit can cause additional damage.

The failure in the material may also be the consequence of cumulative fatigue produced by the repeated impacts of the water jet slugs. During the impact, the shear stress exerted on the coating may deform the upper layer of the coating by stretching the coating from the point of droplet impact. Some coatings, depending on the mechanical properties (e.g. resiliency), may be able to release the stored energy as heat, whereas others will induce small imperfections in the surface by the formation

of small cracks or pits. These failures can enlarge during further exposure. This may be the reason for the erosion of coating B, shown in Figure 2.6(6) and (7). The unexposed coating B, Figure 2.6(5), does not show any visible surface defects (as opposed to coating A).

It was also observed in the experiments that the erosion of a given coating did not start over the entire sample area at the same time, but began in a single point and then spread to the remaining area exposed to water jet impacts. The reason is probably that there are weak points in the matrix resin of the coating that are more sensitive to impacts. This is somewhat similar to degradation of epoxy coatings by sunlight, where damages also spread from weak points in the matrix [43]. Once a defect appears, the erosion can accelerate because of increasing pressures building up on irregularities in the coating surface when water jet slugs impact.

2.7 Conclusions

A new water jet erosion rig that may potentially supplement erosion experiments in the whirling arm apparatus was designed and constructed. The performance of two coating systems, which were also tested in a whirling arm rig, was investigated. The new rig can run with 22 panels simultaneously. The water jet velocity was found to be the most critical parameter for initiation of erosion, though very high velocities (about 167 m/s) were required. Surprisingly, a "matching" of the impact frequency and the impact velocity did not produce similar results in the two setups. In fact, one of the coatings was not damaged, even if the impact frequency of the jet setup was increased by a factor of more than 1300, relative to the whirling arm rig. It was found that original "defects" in the non-exposed coating may act as initiation points and lead to subsequent failure during exposure. Additionally, the cumulative fatigue caused by repeated impacts may induce small imperfections in the surface, leading to visual damage during continued exposure.

In summary, it has, so far, not been possible to directly correlate the results of the whirling arm rig with those of a discrete water jet. Further work will focus on the effects of panel geometry, which are different in the two setups, and the potential significance of the presence of a thin water film on the coating, formed by the previous impacting droplet or jet slug.

2.8 Acknowledgements

Nomenclature

A	the exposed area of coating in unit time t_B (m²)
C	acoustic velocity of water (m/s)
d_h	the gap size of slots in the disk (m)
d_p	the water droplet size in whirling arm test (mm)
f_D	disk rotation frequency (Hz=s⁻¹)
f_j	discrete water jet impact frequency (impacts/m²s)
f_w	impact frequency in whirling arm test (impacts/m²s)
f_{wh}	wheel rotation frequency (Hz=s⁻¹)
l_B	arc length between two adjacent slots in the disk (m)
l_o	amount of rainfall (mm)
l_{wh}	the length of coating exposed area by water jet in unit time t_B
P	water hammer pressure (Pa)
R_D	disk radius (m)
R_{wh}	wheel radius (m)
t_B	the time between two adjacent impacts (s)
t_T	time during which, l_o rain falls (s)
v	impact velocity of water droplets (m/s)
v_D	disk rotation velocity (m/s)
v_j	water jet velocity (m/s)
v_s	steady state sedimentation velocity of rain drops (m/s)
v_w	tip velocity of whirling arm rotor (m/s)
v_{wh}	wheel rotation velocity (m/s)

Greek

φ_w	liquid volume fraction in the whirling arm test chamber (m³ water/m³ chamber)
ρ	density of water (kg/m³)

Subscript

D	disk for chopping jets
wh	wheel for holding sample panels

References for chapter 2

[1] O.G. Engel, Mechanism of rain erosion, Wright Air Development Center, USA. Report No. 53-192 (1953) 1-54.

[2] J.H. Brunton, M.C. Rochester, Erosion of solid surfaces by the impact of liquid drops, in: C.M. Preece (Ed.), Treatise on materials science and technology, Academic press, New York, 1979, 186-248.

[3] S. Wittrup, Vingeforkanter er som dækkene på en bil (in Danish), Weekly Danish newspaper "Ingeniøren" (Nov. 11. 2013) 10-11.

[4] P.S. Veers, T.D. Ashwill, H.J. Sutherland, D.L. Laird, D.W. Lobitz, D.A. Griffin, J.F. Mandell, W.D. Musial, K. Jackson, M. Zuteck, A. Miravete, S.W. Tsai, J.L. Richmond, Trends in the Design, Manufacture and Evaluation of Wind Turbine Blades, Wind Energy. 6 (2003) 245-259.

[5] N. Dalili, A. Edrisy, R. Carriveau, A review of surface engineering issues critical to wind turbine performance, Renew. Sust. Energ. Rev. 13 (2009) 428-438.

[6] C.R. Seward, S.J. Pickles, E.J. Coad, M. Watt, J.E. Field, Studies of rain erosion mechanisms in a range of IR transmitting ceramics - including coated samples, University of Cambridge. Report SPC-92-4032 (1994) 1-206.

[7] G.F. Schmitt, Flight test-whirling arm correlation of rain erosion resistance of materials, Air Force Materials Laboratory, USA. Report AFML-TR-67-420 (1968) 1-31.

[8] C.J. Hurley, G.F. Schmitt, Development and calibration of a mach 1.2 rain erosiion test apparatus, Air Force Materials Laboratory, USA. Report AFML-TR-70-240 (1970) 1-68.

[9] W.F. Adler, The mechanics of liquid impact, in: C.M. Preece (Ed.), treatise on materials science and technology, Academic Press, New York, 1979, 127-185.

[10] C.M. Preece, M.H. Macmillan, Erosion, Annu. Rev. Mater. Sci. 7 (1977) 95-121.

[11] M.B. Lesser, J.E. Field, The impact of compressible liquids, Annu. Rev. Fluid Mech. 15 (1983) 97-122.

[12] M. Lesser, The impact of a compressible liquid, in: M. Rein (Ed.), CISM Courses and Lectures, Springer-Verlag Wien, Vienna; Sachsenplatz 4-6, A-1201 Vienna, Austria, 2002, 39-102.

[13] S. Zwaag, J.P. Dear, S.M. Walley, Rain and solid particle erosion damage mechanisms and materials evaluations, Air Force Wright Aeronautical Laboratory, USA. Report AFWAL-TR-86-4032 (1986) 1-95.

[14] B.S. Mann, V. Arya, An experimental study to corelate water jet impingement erosion resistance and properties of metallic materials and coatings, Wear. 253 (2002) 650-661.

[15] Standard test metod for liquid impingement erosion using rotating apparatus, American Society for Testing and Materials. ASTM G73-10 (2010) 1-19.

[16] G.M.C. Lee, The erosion resistance of plain carbon steels under water droplet impact conditions, Wear. 141 (1990) 185-201.

[17] R.D.R. S.P. Lin, Droplet and spray formation from a liquid jet, Annu. Rev. Fluid Mech. 30 (1998) 85-105.

[18] Y.I. Oka, S. Mihara, H. Miyata, Effective parameters for erosion caused by water droplet impingement and applications to surface treatment technology, Wear. 263 (2007) 386-394.

[19] Y.I. Oka, H. Miyata, Erosion behaviour of ceramic bulk and coating materials caused by water droplet impingement, Wear. 267 (2009) 1804-1810.

[20] Y.I. Oka, H. Hayashi, Evaluation of erosion resistance for metal–ceramic composites and cermets using a water-jet testing apparatus, Wear. 271 (2011) 1397-1403.

[21] M. Grundwürmer, O. Nuyken, M. Meyer, J. Wehr, N. Schupp, Sol–gel derived erosion protection coatings against damage caused by liquid impact, Wear. 263 (2007) 318-329.

[22] P.H. Shipway, K. Gupta, The potential of WC-Co hardmetals and HVOF sprayed coatings to combat water-droplet erosion, Wear. 271 (2011) 1418-1425.

[23] O. Gohardani, Impact of erosion testing aspects on current and future flight conditions, Prog. Aerospace Sci. 47 (2011) 280-303.

[24] M.B. Lesser, Analytic Solutions of Liquid-Drop Impact Problems, Proceedings of the Royal Society of London. Series A, Math. Phys. Sci. 377 (1981) 289-308.

[25] J.E. Field, ELSI conference: invited lecture: Liquid impact: theory, experiment, applications, Wear. 233–235 (1999) 1-12.

[26] O. Gohardani, D.M. Williamson, D.W. Hammond, Multiple liquid impacts on polymeric matrix composites reinforced with carbon nanotubes, Wear. 294–295 (2012) 336-346.

[27] A.A. Déom, A. Luc, S. Amara, D.L. Balageas, Towards more realistic erosion simulation tests for high velocity EM and IR windows, Wear. 233–235 (1999) 13-24.

[28] A. Déom, R. Gouyon, C. Berne, Rain erosion resistance characterizations: Link between on-ground experiments and in-flight specifications, Wear. 258 (2005) 545-551.

[29] M.K. Lee, W.W. Kim, C.K. Rhee, W.J. Lee, Liquid impact erosion mechanism and theoretical impact stress analysis in TiN-coated stream turbine blade materials, Metall. Mater. Trans. A. 30 (1999) 961-968.

[30] C.R. Seward, C.S.J. Pickles, J.E. Field, Single and multiple impact jet apparatus and results, Window and dome technologies and materials. 1326 (1990) 280-290.

[31] E.F. Tobin, T.M. Young, D. Raps, O. Rohr, Comparison of liquid impingement results from whirling arm and water-jet rain erosion test facilities, Wear. 271 (2011) 2625-2631.

[32] B. Luiset, F. Sanchette, A. Billard, D. Schuster, Mechanisms of stainless steels erosion by water droplets, Wear. 303 (2013) 459-464.

[33] M. Ahmad, M. Casey, N. Sürken, Experimental assessment of droplet impact erosion resistance of steam turbine blade materials, Wear. 267 (2009) 1605-1618.

[34] J. Zahavi, S. Nadiv, G.F. Schmitt Jr., Indirect damage in composite materials due to raindrop impact, Wear. 72 (1981) 305-313.

[35] C.J. Hurley, J. Zahavi, G.F. Schmitt Jr., UV radiation exposure effects on the rain erosion resistance of coated monolithic poly(carbonate) transparencies, Wear. 87 (1983) 9-28.

[36] W.F. Adler, Particulate impact damage predictions, Wear. 186–187, Part 1 (1995) 35-44.

[37] C. Westmark, G.W. Lawless, A discussion of rain erosion testing at the United States Air Force rain erosion test facility, Wear. 186–187, Part 2 (1995) 384-387.

[38] W.F. Adler, Rain impact retrospective and vision for the future, Wear. 233–235 (1999) 25-38.

[39] Protection from wind and weather: rotor blades of wind turbines with chemicals by BASF, http://www. basf-coatings. com/global/ecweb/en/ (Accessed 20.12.2013).

[40] M. Lesser, Thirty years of liquid impact research: a tutorial review, Wear. 186–187, Part 1 (1995) 28-34.

[41] M H Keegan and D H Nash and,M.M.Stack, On erosion issues associated with the leading edge of wind turbine blades, J. Phys. D. 46 (2013) 383001.

[42] A. Sareen, C.A. Sapre, M.S. Selig, Effects of leading edge erosion on wind turbine blade performance, Wind Energy (2013). DOI: 10.1002/we.1649.

[43] S. Kiil, Model-based analysis of photoinitiated coating degradation under artificial exposure conditions, J. Coat. Technol. Res. 9(4) (2012) 375-398.

[44] B.J. Briscoe, M.J. Pickles, K.S. Julian, M.J. Adams, Erosion of polymer-particle composite coatings by liquid water jets, Wear. 203–204 (1997) 88-97.

Chapter 3 - Rain erosion of wind turbine blade coatings using discrete water jets: effects of water cushioning, substrate geometry, impact distance, and coating properties

This chapter is prepared for submission for publication in Wear with the title "Rain erosion of wind turbine blade coatings using discrete water jets: effects of water cushioning, substrate geometry, and coating properties" (authors Shizhong Zhang, Kim Dam-Johansen, Pablo L Bernad Jr., Søren Kiil)

3.1 Abstract

Rapid and reliable rain erosion screening of blade coatings for wind turbines is a strong need in the coatings industry. One possibility in this direction is the use of discrete water jets, where so-called jet slugs are impacted on a coating surface. Previous investigations have mapped the influence of water jet slug velocity and impact frequency. In the present work, the effects on coating erosion of water cushioning, substrate curvature, and water nozzle-coating distance were explored. The investigations showed that in some cases water cushioning (the presence of a liquid film on the coating surface prior to impact) influences the erosion. Contrary to this, substrate curvature and the water nozzle-coating distance (< 10 cm) did not influence the results to any significant degree.

Mechanical measurements to characterize selected blade coatings, including tensile strength, flexibility, impact, hardness, and abrasion experiments, were also conducted. The ranking of abrasion resistance of the blade coatings was in agreement with the ranking of rain erosion resistance measured in the whirling arm rig (an industrial standard).

Results of this work, with more pertinent parameters explored, confirm the conclusion from our previous investigation that a direct correlation of data from discrete water jet experiments with those obtained in the whirling arm rig does not seem possible. The underlying mechanisms of rain erosion are substantially different in a setup based on impacting water jet slugs and a setup where a rotor arm impacts falling water droplets.

3.2 Introduction

During service life, the blades of wind turbines are exposed to continuous impacts with rain droplets, hail, insects, or solid particles (e.g. sand) carried by the wind. This can lead to erosion of the blades, whereby the electrical efficiency and weight balancing are reduced and expensive repairs may be required. This is particular problematic offshore, where access time, due to bad weather, can be limited and maintenance in general is very expensive. Blade tip velocities on modern wind turbines can get close to 100 m/s and means to protect the blades from (rain) erosion are required. One possible solution is somewhat elastic blade coatings, which are able to absorb the impact energy without crack formation [1-4]. Crude estimations in the industry suggest that about 50 % of new large (>3 MW) wind turbines are specified with blade coatings.

Fast, reliable, and cost effective evaluation of new blade coating formulations is essential. Presently, the industrial standard, the so-called whirling arm rig, is mostly used for experimentation [1]. It consists of a rotor, 2 m in diameter, rotating in an imposed artificial "heavy" rainfall. Experimentation time is about three hours, and rotor tip speeds up to 150 m/s are used. However, a fast-working, laboratory-size screening device that can be used directly in the coating companies to evaluate many samples simultaneously is highly desired. A variety of experimental erosion rigs, mainly aimed at materials for aircrafts, have been designed and constructed in the past 100 years or so and were reviewed in [1].

In our earlier work [1], a setup based on discrete water jet slugs was presented and the effects on erosion of water jet slug velocity and droplet impact frequency were investigated. An important observation was that micrometer-size coating defects, present prior to experimentation, appears to play an important role for the erosion mechanism. Another finding for the two coating types investigated, under conditions where impact frequency and water hammer pressure are "matched", was that results could not be directly correlated with those obtained in the whirling arm rig. In the present work, additional experiments have been conducted with water jet slugs in pursue of a correlation between the two setups. Parameters investigated are water cushioning, substrate curvature, and water nozzle-coating distance. Measurements of mechanical coating properties, including tensile strength, flexibility, impact, hardness, and abrasion experiments, to characterize blade coatings, were also conducted.

The purpose has been to focus on testing methodology and to correlate erosion results with selected mechanical properties. More detailed studies of the localized mechanisms of rain erosion were beyond the scope of the work.

3.3 Mechanisms of liquid erosion

The underlying mechanisms behind drop impact erosion involve interactions of several stress (pressure) waves in combination with successive drop impacts. A schematic illustration of a single water drop impact is shown in Figure 3.1.
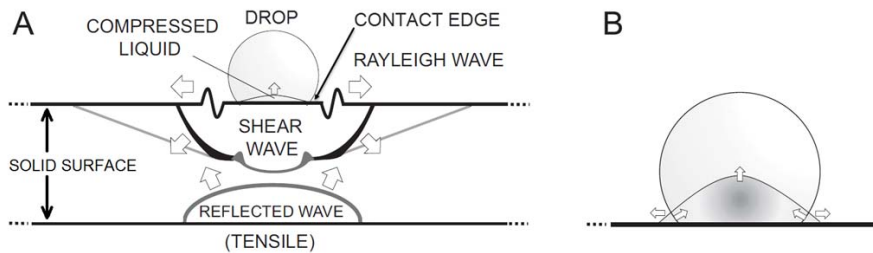

Figure 3.1 Schematic drawing of liquid droplet and rigid solid surface impact interaction. (A) shows the three main waves generated by the impact and (B) shows the deformation (outflow) of the compressed droplet. Reproduced from [8] with permission from Elsevier.

The failure, caused by impact, is divided into two regimes [5]. One occurs at the very impact site and may initiate material deformation and cracks in the surface. The other takes place when high velocity lateral water jets tear away any unevenness in the surface material near the impact site [5].

The first damage can occur when the contact (drop-surface) edge travels across the impacted surface (horizontally in Figure 3.1) at a velocity greater than that of the reflected (shock) wave propagating into the water drop [Figure 3.1 (A)]. Due to lack of a free surface where the pressure can be released, the water behind the shock front is compressed and energy stored. Under the impact conditions considered here, the pressure exerted on the target surface is known as the water hammer pressure and is a function of the liquid density and impact velocity. It can cause direct cracks in the coating surface. The impact pressure may reach values three times the central water hammer pressure [6,7].

Later in the impact event, the second stage of the erosion mechanism sets in. The contact edge between the target surface slows down and is overtaken by the shock

front [5]. Thereby, water trapped in the compressed region can escape, which generates water jets (Rayleigh wave) across the surface causing a high velocity sideways jet of fluid. Irregularities greater than 100 nm, originating from surface roughness or damage, can be torn away resulting in material loss or further extension of cracks. In total, there are three stress waves generated in the surface by the impact: compression wave, shear wave and Rayleigh surface wave (see Figure 3.1). The compression wave has little effect on the damage pattern. The overall interaction of these waves can be complex and depends upon impact conditions and material properties [8]. Details are available in other sources e.g. [8].

The complex phenomena described above suggest that the contact mode, when experimenting with rain erosion, can be very important. In this work, focus is on the fundamental difference between movement of coated panels against rain drops (i.e. whirling arm rig) versus movement of water drops against coated panels (i.e. discrete water jets).

Another aspect that is central for the work presented in subsequent sections is that of so-called "water cushioning", which refers to a potential lower erosion rate of a wetted compared to a dry surface. In the case of wind turbine blade coatings under natural exposure, a water film, originating from an impacting drop, might not be allowed to form, will exist for a very short time only, or be very thin because of the high tip speeds prevailing, which force-blows away any residual water. However, in any water drop erosion setup based on static, or almost static, coated panels (such as the ones of this work), a thin water film is indeed expected to form and be present when consecutive water drops impact. In both cases, the shattering of water drops into thousands of smaller drops, which are sent in all directions, must also be kept in mind. In mechanistic terms, a water film can be formed when the rate at which liquid arrives at the surface is high enough to balance the losses due to air friction, rotational removal, and water evaporation. Brunton and Rochester [9] have suggested two reasons why the presence of a liquid film might reduce rain erosion damage of a surface: (i) When it is struck by a water drop, the liquid film deforms, so that the pressure on the surface is less than it would have been if the surface had been dry. However, the effect will only be significant if the liquid film thickness is above a certain critical value (not quantified). (ii) The impact pressure is reduced because the pressure wave diverges as it passes through the liquid layer. If the layer is thick

compared with the diameter of the drop, attenuation will vary as the square of the layer thickness.

3.4 Strategy of investigation

In this experimental study, the following rig parameters are investigated: the water cushioning effect, the geometry of coating samples, and the nozzle-coating distance. The water cushioning effect is evaluated by incorporating an air nozzle that can, fast and continuously, remove the water film formed upon droplet impact on the coating surface. To investigate the effect of coating panel geometry (curvature), steel panels with the shape of a wind turbine blade (leading edge), normally used for the whirling arm erosion rig, were used. For the nozzle-coating distance effect, the length between the water jet nozzle orifice and the coating panel was decreased by 50 % (relative to the distance of 10 cm used in earlier work).

In an attempt to correlate physical coating properties with erosion performance, three blade coatings, with different behaviors in the whirling arm experiment, were thoroughly characterized and two of them used in the water jet experiments.

3.5 Experimental procedures

3.5.1 Modification of water jet erosion rig

In a previous publication [1], the design and construction of the water jet erosion rig were described in detail. Only a summary of the major features and operating parameters of that equipment is provided here. The basic configuration is shown in Figure 3.2.
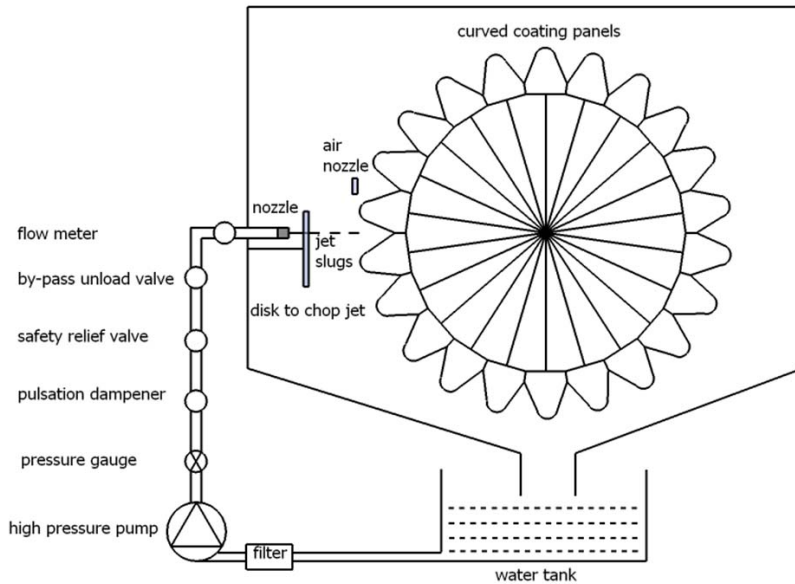
Figure 3.2 Schematic illustration of water jet erosion rig after modification with curved coating panels. Details of the setup are provided in [1].

The basic principle is a water jet, driven by a high pressure pump. The jet generated is dependent on the nozzle type and angle used. Tap water is used as the eroding liquid for all the experiments. The standard distance of nozzle orifice to coating sample surface is 10 cm. The water can be recycled from a hold up tank and reused after filtration. A thermostated water bath is used to control the water temperature. The moving wheel (diameter of 52 cm) in the middle of the chamber, holding up to 22 coated steel panels, is driven by an electronic motor, allowing for various rotation velocities (0.1-4.5 RPM). The water flow rate can be varied. A rotating stainless steel disk (diameter of 10 cm), with 10 mm holes or 1 mm slots, is used to chop the continuous straight water jet into slugs. Erosion is evaluated by inspecting samples at predetermined time intervals. The potential erosion damage was recorded every 5 hours when using the 1 mm disk. For the experiments with the 10 mm disk, erosion was much more aggressive and inspection was conducted every 10 min in the early phase and at longer times every 2 hours. Erosion failure is defined by the incubation time of the coatings, defined here as the time period prior to erosion damage appearing. A number of modifications to the original setup have taken place and will be discussed in the coming sections.

3.5.1.1 Water cushioning

To evaluate the water cushioning effect, blade coatings applied on flat steel panels with dimensions 7.0×15.0 cm and a thickness of 2 mm were used for erosion experiments. A separate air nozzle using pressurized air at 2 bars was incorporated into the rig. The air flow from the nozzle points in direction to the small area where the water jet slugs impact as shown in Figure 3.3. This ensures that the water film formed on the coating surface upon droplet impact can be rapidly removed; thereby simulating what takes place on a real wind turbine blade moving at high velocities. The water film removal was verified by visual inspection.
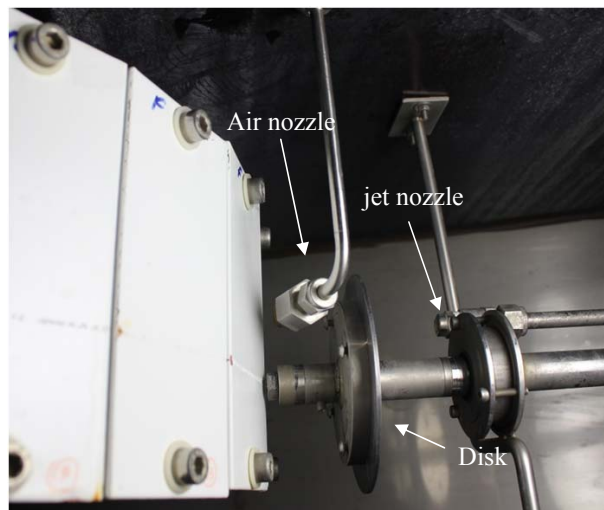

Figure 3.3 Photo showing the position of the air and water nozzles in the rig. The white panels to the left are blade coating samples attached to the large, slowly rotating, wheel.

3.5.1.2 Sample geometry

In the whirling arm experiment, coating samples, simulating the leading edge curvature of wind turbine blades, are used. Contrary to this, in our previous water jet experiments [1], flat steel panels were used. The geometry (curvature) may have an effect on the erosion behavior of the coatings and therefore the effect of this parameter was investigated. Suitable curved panels were obtained simply by using the metal substrates from the whirling arm rig. A close-up photo of these substrates can be seen in Figure 2.4 in [1], and a schematic illustration of their placement in the water jet rig is shown in Figure 3.2.

3.5.1.3 Impact distance

To evaluate the effect of jet nozzle-coating gap, the distance was decreased from 10 to 5 cm. Experiments were based on coated flat steel panels of dimensions 7.0×15.0 cm, in the presence of air blowing.

3.5.2 Details of coating samples used in erosion experiments

3.5.2.1 Samples for cushioning effect and impact distance experiments

Flat steel panels of dimensions 7.0×15.0 cm and a thickness of 2 mm were used as substrate. They were firstly coated by an epoxy primer followed by two different polyurethane-based blade coatings (topcoats), termed coatings A and B. Both coatings contain xylene and polar solvents (butyl acetate type). The binder of coating A consists of a common commercial polyester polyol cured with a common commercial flexibilized isocyanate trimer. For Coating B, the same polyester polyol as for coating A was used and the curing agent was a standard isocyanate trimer. Both coatings contain colouring pigments (mainly TiO_2) and standard extenders.

A hole was drilled at each end of the panel allowing for attachment to the moving wheel. Coating application was done using airless spray at 200 bars and coatings cured at 23 °C for 7 days. The total DFT of primer and topcoats, measured using an Elcometer Model 355 Top, calibrated for 500 µm thickness, was 517.0±51.6 µm for the coating A system based on 13 separate samples and 349.0±39.4 µm for the coating B system (also 13 separate samples). The panels used for water jet nozzle-coating distance experiments had a total film thickness of 508±50.2 µm for Coating A based on 3 samples and 369.5±40.0 µm for Coating B based on 3 samples.

3.5.2.2 Samples for curvature effect experiments

The special curvature of the panels was established prior to coating application. The curved panel was first coated by a primer and then a topcoat (either Coating A or B). Coating application was done using airless spray at 200 bars and cured at 23 °C for 3 weeks. The total DFT of primer and topcoats was 454.0±25.9 µm for the coating A system (3 replicates) and 413.0±18.5 µm for the coating B system. The length of a coated test sample is 22.5 cm.

3.5.3 Investigation of physical properties of coatings

Physical properties of interest for blade coatings are: (1) tensile strength experiments, to investigate the stress-strain behavior of coatings. (2) Pendulum damping experiments, to investigate the hardness based on the principle that the amplitude of the pendulum's oscillation will increase when supported on a harder surface. (3) Mandrel bending experiments, to investigate the extent to which it resists deformation (cracking) in response to an applied force. (4) Taber abrasion experiments, to investigate the abrasion resistance of coatings, and (5) impact experiments, to investigate the resistance of coatings to the effects of rapid deformation.

A third coating sample, coating C (also polyurethane- and solvent-based), was included to expand the mapping of properties against erosion behaviour. The binder of Coating C was a common commercial acrylic polyol cured with a standard isocyanate trimer. Coating C was not evaluated in the water jet setup, but past experience has shown that its performance in the whirling arm setup is poor in comparison to coating B. Coating A performs better than coating B in the whirling arm rig.

In the subsequent sections, all coating sample preparations and subsequent curing were done at a temperature of $23\pm2°C$ and a relative humidity of $50\pm5\%$.

3.5.3.1 Stress-strain (tensile strength)

The tensile strength experimentation is based on ASTM D 2370-92. It was performed using a Zwick Universal Testing Machine Z2.5/TS1S-2000 equipped with load cells providing up to 500 N. The three coatings were applied on thin plastic foils and cured for 3 weeks. Coated foils were cut into a strip dimension of 30 ×100 mm before removing the coating films from the special backing foil. This was done to minimize the risk of damaging the edges of the strips. 10 replicate strips were prepared for each coating. The thickness of each coating was measured before the experiments. Coating C formed a rather brittle film on the foils, not very suitable for tensile strength experimentation, and only Coating A and B could be used. Before operating the equipment, a strip was placed and aligned between the two "jaws" used for fixation of the test specimen. The lower jaw was kept static and the upper one moved at a predetermined displacement velocity. For all films investigated, the maximum displacement velocity of 100 mm/min was chosen. Young's modulus (material

stiffness) was estimated from the linear part of the stress-strain curves (elastic region at low strains).

3.5.3.2 Mandrel bending experiments

The three blade coatings were applied on steel panels of dimension $70 \times 150 \times 0.8$ mm, and cured for 3 weeks. To conduct the experiment, a coated panel was inserted and clamped into the conical mandrel (model Erichsen 312), and was bent in an even movement through 180º in about 1 s. Three replicate panels were used for each coating. Elongation at break was calculated according to ASTM D522. The bent panel was evaluated using optical microscopy (10x magnification): the crack farthest away from the small end of the conical mandrel was marked and the distance from the farthest end of the crack to the small end of the mandrel was measured. The average distance of 3 replicate panels was used to determine the percent elongation. The film thickness was measured before the experiment and all experiments were conducted at the same controlled temperature (23 ± 2 °C) and relative humidity ($50 \pm 5\%$).

3.5.3.3 Impact experiments

Impact experiments were performed using an Erichsen variable impact tester model 304 following ASTM D2794. Coating A, B and C were applied on steel substrates with dimension $200 \times 300 \times 1.5$ mm and cured for 3 weeks. To perform the impact test, the coated panel was placed on the support with a hole of 16.3 mm and a falling hemispherical impact head (15.9 mm diameter, 453.6 g weight) was then allowed to impact the coating and substrate centered under the indenter. The impact is on the coating side and the indentation in this case is an intrusion. When the indenter strikes the panel it deforms the coating and the substrate. By gradually increasing the distance the weight drops, the point at which failure occurs can be determined. The impact strength value is recorded as the highest impact energy which results in no visible cracks and detachment of the film.

3.5.3.4 Pendulum hardness experiments

The pendulum hardness experiment is based on the principle that the amplitude of the pendulum's oscillation is dependent on the hardness of the surface. The harder the surface, the greater the amplitude of pendulum oscillation. A König pendulum

hardness tester (Sheen Instruments Ltd, UK) was used to measure the surface hardness of the cured film. The three coatings were applied on glass panels with dimension 100×150 mm and cured for 7 days. The pendulum oscillation times from 6º to 3º was measured at the same temperature and humidity as the curing. The measurement was repeated at three different positions. The DFT was measured before the experiment.

3.5.3.5 Taber abrasion experiments

Experiments of abrasion resistance of the three coatings were conducted according to ASTM D4060-10. Three coatings were applied on steel substrates with dimension 100×100 mm, and cured for 3 weeks. Three replicates of each coating were prepared and DFT was measured. The experiment was performed using Taber 5130 abraser with the abrasive wheel CS-17. To perform the experiment, the panel was first weighted and then mounted on the horizontal turnable platform. The surface was abraded by rotating the panel under 1 kg load abrasive wheels for 500 cycles. The platform rotated at a speed of 1 cycle per second. After exposure, the panels were gently brushed to remove any residual dust and abradings and then weighted. Afterwards, the panel was put back in the platform for further 500 cycles of abrasion.

3.5.3.6 Other relevant characterization methods

Another coating parameter of interest is the relaxation time. As discussed by Conn [9], repeated impacts can accumulate stresses in a coating until it fails. If the relaxation time of the coating is short, relative to the time between two successive impacts, the coating may be able to regain its impact absorption capability (resilience) between two impacts and show good performance as a blade coating. On the other hand, if the relaxation time is too long, stresses can accumulate and failures occur. The pertinent relaxation times during rain erosion are of the order of 1-3 µs [9], which are very difficult to measure. Conn [9] has done investigations with relaxation times of about 100 µs.

3.6 Results and Discussion

A series of experiments was conducted using the water jet setup. Two blade coatings, termed A and B, were selected for the investigation. The results are summarized in Table 3.1. An experimentation time of 66 hours with 22 sample positions on the

moving wheel, corresponds to three hours of exposure per sample in the whirling arm rig [1].

Table 3.1 Overview of process parameters and results for experiments in water jet erosion rig. The result "Coating B > Coating A" means that the performance of coating B was better than that of coating A. Three replicates were used in each of the experiments (1-4). The results under damage description were the same for all samples in each experiment. Experiments 1-6 were all conducted with a nozzle diameter of 0.84 mm, a discrete straight jet, and a jet velocity of 167 m/s (150 bar).

Experiment No.	Purpose of experiment	Coated panel shape	Comparison with exp. no.	Disk gap size (mm) d_h	Disk rotation (rpm) f_D	Wheel rotation (rpm) f_{wh}	Nozzle-coating distance (mm)	Air blowing	Exp. time (hrs)	Damage description	Result (ranking)
1	Effect of water cushioning	Flat	5	1.0	840	4	100	Yes	132	Coating B started pitting in 58 hrs Coating A no damage in 66 hrs	Coating A > Coating B
2	Effect of water cushioning	Flat	5	1.0	840	4	100	Yes	132	No erosion for both samples	Coating A =Coating B
3	Effect of sample shape	Curved	4	10.0	420	4.5	100	Yes	10	Coating A eroded in 30 mins, Coating B eroded in 10 hours	Coating B > Coating A
4	Effect of impact distance	Flat	6	10.0	420	4.5	50	Yes	16	Coating A eroded in 20 mins, Coating B eroded in 16 hours	Coating B > Coating A
5	Data from [1]	Flat	-	1.0	840	4	100	No	66	Coating A started pitting in 25 hrs Coating B no damage in 66 hrs	Coating B > Coating A
6	Data from [1]	Flat	-	10	420	4.5	100	No	3	Coating A started pitting in 1/3 hrs Coating B no damage in 3 hrs	Coating B > Coating A

3.6.1 Effects of water cushioning

As discussed in section 3.3, when using a continuous or discrete water jet to impact coated panels, the potential presence of a thin water film on the coating surface may influence the results. The water film is formed when the preceding water jet slug

impacts the surface. In contrast, a wind turbine blade moving through air at high speeds may blow away the water film and instead establish an air film. This so-called "water cushioning effect" may reduce the erosion damage on a material as noted by Brunton and Roschester [9] and could potentially also influence the relative performance of different blade coatings. Experimentation is needed to quantify the behavior.

In the replicate experiments on this effect (experiment 1 and 2, see Table 3.1), the water film was blown away using an air nozzle. Experiment 1 showed no erosion of coating A, even after 132 hours of experimentation. Contrary to this, coating B began to show some pitting after 58 hours. This coating ranking is in good agreement with data from the whirling arm rig [1]. After 102 hours, the damage observed was a small hole with a diameter of about 1 mm and a crack "attached" to the hole as shown in Figure 3.4 (1). After an additional 5 hours exposure in the discrete water jet, the periphery of the crack was eroded as seen in Figure 3.4 (2). In the subsequent 5 hours of exposure, the crack developed and formed a new pitted area as shown in Figure 3.4 (3).
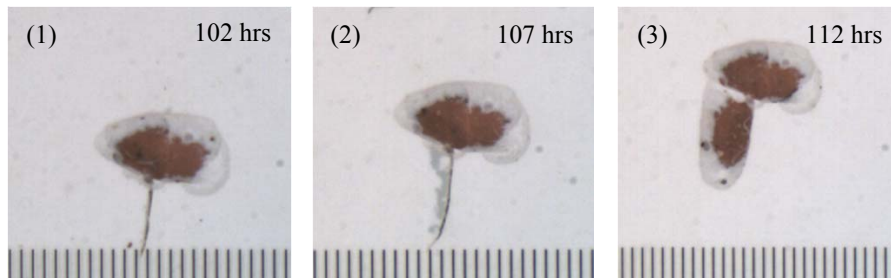

Figure 3.4 Optimal microscopy showing rain erosion damage development of Coating B (Experiment 1). The scale at the bottom is 0.1 mm between two vertical lines.

Experiment 2 was conducted to verify Experiment 1. Fresh panels of Coating A and B were tested in the water jet rig and the experimental parameters kept the same. However, the new panels of both Coating A and B showed no sign of erosion in 132 hours and the erosion performance of Coating B in Experiment 1 could therefore not be repeated. This suggests that a weak spot, present only in the first version of Coating B somewhere in the small area exposed to the water jet, led to the failure observed. This hypothesis is in agreement with Figure 2.6 in [1], where it was shown

(for coating A) that cracking initiates from defects already present in the non-exposed coating. In summary, damages may develop from an existing imperfection or from a damage induced by cumulative fatigue under continuous impacts.

A previous experiment from [1] (included as Experiment 5 in Table 3.1), using the same process parameters as in Experiment 1 and 2, but in the absence of any air blow showed erosion of coating A in 25 hours). Since no erosion of coating A appeared in Experiment 1 and 2 in the present work (even after 132 hours of exposure), the air blow has an effect, at least for coating A. Apparently, water cushioning accelerates erosion, but the actual mechanism cannot be deduced from the present limited data set. This observation is rather surprising in light of the discussion in section 3.3 where it was mentioned that other researchers have seen the opposite effect for water drop erosion on steam turbine blades. However, this may be attributed to the physical conditions. Brunton and Roschester [9] used rotating blades and radial flow, whereas the setup of this work is based on jet slugs on slowly moving panels. It is recommended to use the air nozzle in water jet experiments because this situation is closer to both whirling arm and real blade coating exposure.

3.6.2 Effect of sample curvature

The effect of substrate curvature was evaluated using curved panels as shown schematically in Figure 3.2. Experiment 3 in Table 3.1 was conducted to evaluate the curvature effect. Note that the disk gap size in this case is higher than in Experiment 1 and 2, corresponding to longer and heavier jet slugs and thereby a more aggressive exposure. For comparasion with Experiment 3, Experiment 4 with a flat panel should be considered. Note that the nozzle-coating distance is not the same in Experiment 3 and 4 (100 and 50 mm, respectively), but as shown in a later section, the erosion results are the same for those two (small) nozzle-coating distances. In both Experiment 3 and 4, air blowing was included.

For Experiment 4, using flat steel substrates, coating A eroded in 20 min, whereas coating B eroded in 16 hours. Experiment 3, using curved steel substrates, gave similar results with erosion of coating A after 30 min and erosion of coating B after 10 hours. For Experiment 3, the erosion of Coating A (three replicates) initiated in the middle of the convex surface where the water jet impacts the panel from a perpendicular direction (see the setup in Figure 3.2). The failure type in the three identical Coating A samples are small pits as shown in Figure 3.5, and the damage

repeatable. In summary, Coating B is superior to coating A with respect to erosion and substrate curvature does not change this ranking. The ranking obtained is not in agreement with results from the whirling arm rig (for details of those results see [1]) and the mechanisms of erosion must therefore be of a different nature for the two coatings considered in the erosion experiments.
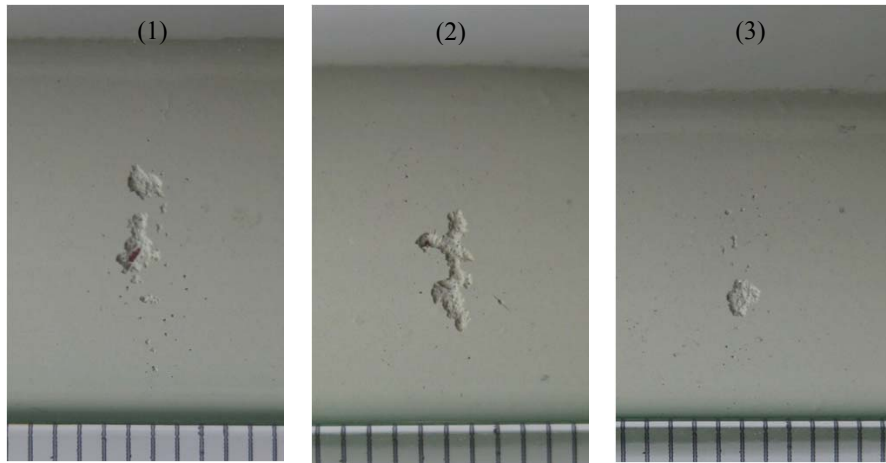

Figure 3.5 Digital camera photos of water jet erosion damage of Coating A when using curved panels (Experiment 3). Photos were taken after 30 minutes of experimentation. (1)-(3) refer to repititions. The scale at the bottom is 1 mm between two vertical lines. In photo (1), the red underlying primer is visible in the large pit and the damage has penetrated the blade coating.

3.6.3 Effect of impact distance

The distance from the water jet inlet (nozzle) to the coating surface is another process parameter of interest. It is expected that reducing this distance may increase the rate of erosion significantly because air friction slows down the water jet slugs. The distance was decreased from 10 to 5 cm in the presence of air blowing (other conditions are shown in Table 3.1, Experiment 4). It was found that Coating A started pitting in 20 minutes (see Figure 3.6), whereas Coating B showed no sign of erosion for the first 16 hours.

Figure 3.6 Optical microscopy of water jet erosion failure of Coating A applied on flat steel panels and using a water nozzle-coating distance of only 5 cm (Experiment 4).

The time and type of failure and the performance ranking are consistent with the experiments conducted at an impact distance of 10 cm presented in our earlier work [1]. The explanation for this result is probably that both 5 and 10 cm impact distance is very short. Increasing to distances higher than 10 cm will, at some critical distance, result in less or no erosion, but that is not of vital interest for this work and it was not investigated further.

3.6.4 Characterization of coatings

To enable a scientific understanding of the erosion behaviours of the different coatings, various mechanical experiments were conducted to characterize the coatings. All three coatings are polyurethane-based top coats and contain pigments. When evaluated in the whirling arm rig, the ranking was (best performing coating first): Coating A > Coating B > Coating C. It is not known if these whirling arm data correlate with natural (real life) data, but it is an underlying assumption. Due to the very long constants of natural exposure, it has not been possible to test that assumption in this work.

3.6.4.1 Stress-strain behavior of blade coatings

Table 3.2 Average (10 replicates) stress-strain data for Coating A and B. Strain is defined as the ratio of the change in length of the sample to its original length.

n =10	Coating Samples	Strain at Fmax (mm)	Strain at break (%)	Ultimate tensile Strength (MPa)	Young's Modulus (N/mm^2=MPa)
$\bar{x}$	Coating A	96.49±7.07	96.49±7.07	7.13±1.32	12.19±1.95
	Coating B	75.18±4.76	75.18±4.76	9.52±0.78	17.93±0.48

The average tensile strength experimental data of 10 replicate samples of Coating A and B are shown in Table 3.2. For both coatings, it can be observed that the maximum strain and strain at break are the same. The fracture happened at the maximum strain value.

Coating A has a strain value of 96.49 %, which is higher than that of Coating B, measured to 75.18 %. This means that Coating A has a better ability to resist shape changes without crack formation. Coating B is found to be less elastic than Coating A as evidenced by the Young's modulus values, though the difference is not large. By comparing the ultimate tensile strength, it can be found that less force is needed for Coating A to fracture. Young's modulus at ambient temperature for an epoxy adhesive is about 2461 MPa [10] and that of rubber is 10-100 MPa [11]. In comparison, the blade coatings have a Young's modulus similar to rubber. In the whirling arm rig, Coating A has better erosion resistance than Coating B.

3.6.4.2 Mandrel bending experiment (flexibility)

Blade coatings must have a certain degree of flexibility. This can be of relevance for droplet impacts, but also during start up and shut downs of the wind turbine where the blades are somewhat displaced from their equilibrium position. Strong winds may also displace the blades. The mandrel experiment can help estimating how resistant a coating is to cracking and detachment from the substrate. The average DFT of Coating A, B, and C was 243, 209, and 151 μm, respectively. Coating A and B showed no cracking or detachment at all. Coating C, however, showed cracking at scale 2 as shown in Figure 3.7. The elongation at break was found to be 8.1%. In summary, Coating C exhibited least cracking resistance compared with Coating A and B and a similar performance ranking was found in the rain erosion experiment

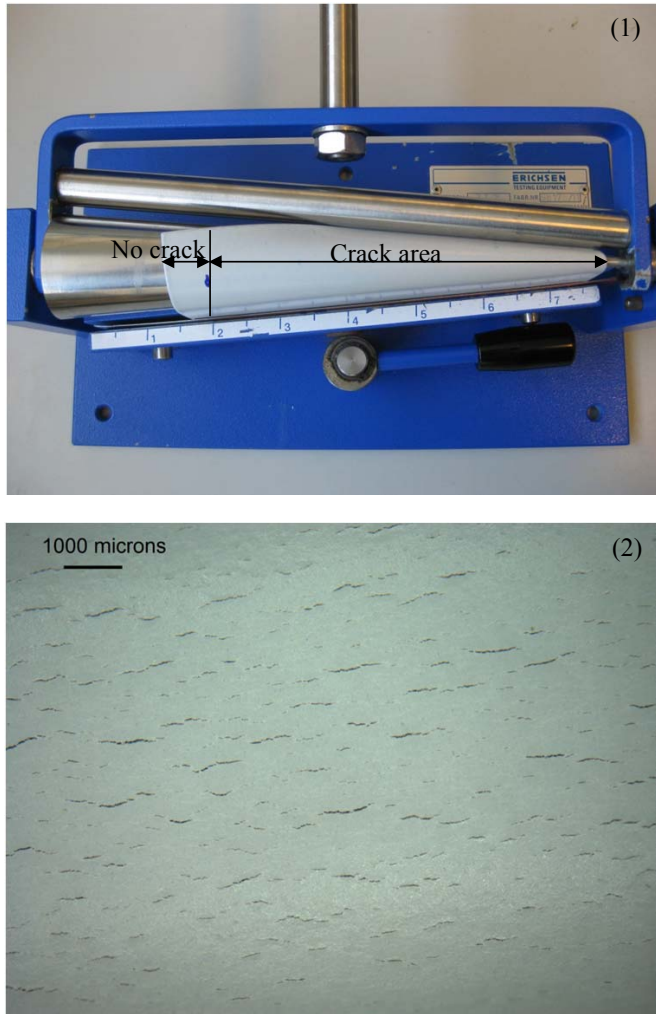(whirling arm rig). This is an indication that coating flexibility may be an important parameter for blade coatings.

Figure 3.7 (1) Mandrel bending test equipment, (2) Optical microscopy of cracking of Coating C.

3.6.4.3 Impact experiments

Impact experiments are relevant for blade coatings because of the occasional collisions with airborne solid particles, hail, birds, and insects during its service life. The average DFT of Coating A, B, and C was 370, 380, and 375 μm, respectively. Coating A and B showed no sign of cracking or detachment even when impacted with

the maximum energy of 14.5 J. Coating C, however, detached from the substrate at an impact energy of only 2.6 J. Photos of the performance of the three coatings are shown in Figure 3.8. The ranking of impact resistance is Coating B = Coating A > Coating C. This suggests that Coating A and B both limit the chance of impact induced failures such as cracking and detachment, which can give weak spots for further erosion by rain droplets.
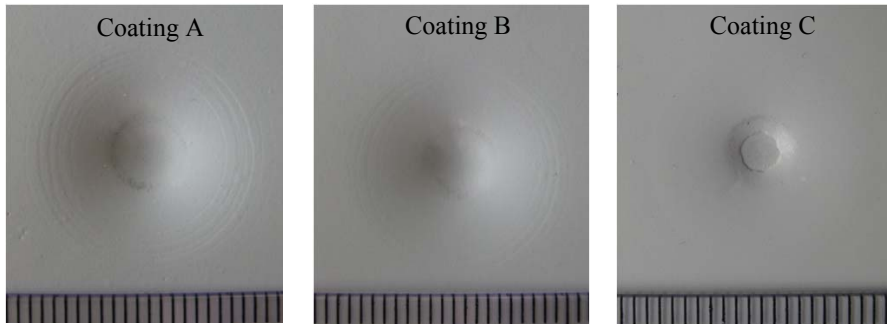

Figure 3.8 Digital camera photos of impact damages of the three non-exposed blade coatings. The scale at the bottom is 1 mm between two vertical lines.

3.6.4.4 Pendulum hardness test

Another parameter of interest is the hardness of the blade coatings. It is generally believed that blade coatings should not be too hard because the ability to absorb rain droplet energy (resiliency) will then be compromised. Here, the pendulum hardness is investigated over time. In Figure 3.9, the change in surface hardness, expressed as oscillation times versus time, is shown.
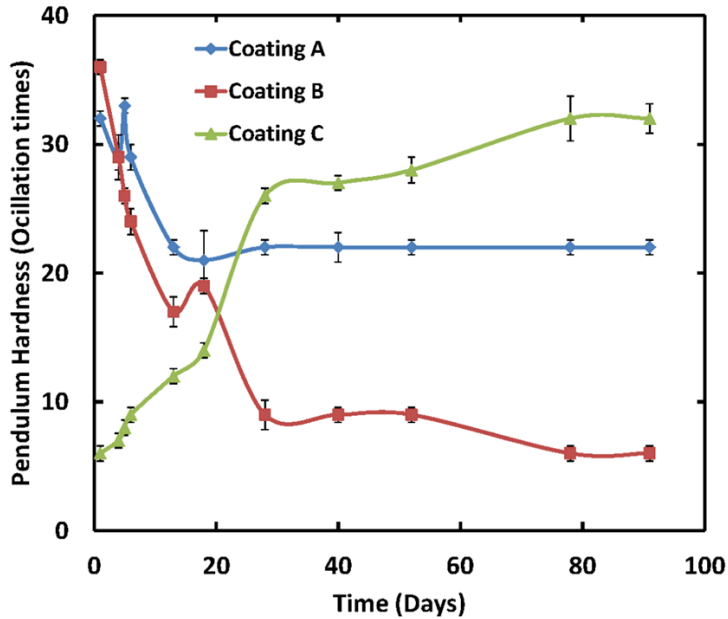
Figure 3.9 Measurements of pendulum hardness for the three blade coatings over time.

The average DFT of Coating A, B, and C was 290, 270, and 240 μm, respectively. The experiment ran over 91 days. Initially, it was found that Coating A and B had very similar pendulum hardness while Coating C had a softer surface to begin with. However, the hardness of both Coating A and B declined fast in the first about 20 days to reach a more or less constant value, while the Coating C hardness increased rapidly and after about 25 days exceeded the hardness of both Coating A and B. Coating C also reached a more or less constant value after about 25 days. The behavior observed could be due to residual solvent contents of the coatings [12], which may be released during the first 20-30 days. The steady state values show that Coating C has the highest hardness value followed by Coating A and finally Coating B. This ranking is in agreement (softer is better) with the water jet erosion ranking (only Coating A and B were investigated). However, it is not in agreement with the whirling arm ranking, where coating A did best, so it is not possible to reach a conclusion on any correlation between pendulum hardness and rain erosion resistance.

3.6.4.5 Taber abrasion experiments

Abrasion resistance is a relevant parameter to explore because blade coatings may not only crack and delaminate during rain erosion, but also simply suffer from a steady thickness reduction over time. Results are shown in Figure 3.10, and it can be seen that Coating A has better abrasion resistance than Coating B (about 10 times higher after 1000 cycles) even though the absolute values in both cases is rather small. Coating C, on the other hand, has a much higher weight loss (about 13 times higher than that of Coating B). This ranking of abrasion resistance, Coating A > Coating B > Coating C, is in perfect agreement with the whirling arm rain erosion results. It would be interesting (but expensive) to explore this correlation on a much larger data set.
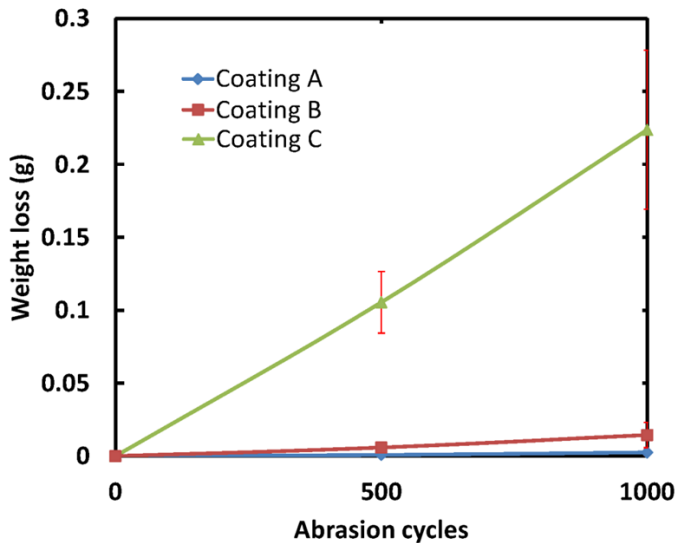

Figure 3.10 Weight loss data for the three blade coatings when exposed to abrasion cycles.

3.7 Conclusions

A series of experimental investigations with a new water jet erosion rig has been performed. In particular, the effects on coating erosion of water cushioning, substrate curvature, and water nozzle-coating distance were investigated. The main results are:

1) Water cushioning can be of importance at not too aggressive conditions and it is recommended to include air blowing when using water jet slugs to simulate rain erosion.

2) Substrate curvature does not influence erosion rate and flat panels, which are easier to handle during practical preparations, can be used.

3) The water nozzle-coating distance (< 100 mm) does not affect the erosion rate.

Several mechanical experiments to characterize blade coatings were also conducted. Abrasion resistance appears to be an interesting property to correlate with rain erosion data. The ranking of coatings from this particular test method was in agreement with the ranking based on rain erosion rate data from the whirling arm rig.

Results of this work, with more pertinent parameters explored, confirm the conclusion from the previous investigation that a direct correlation of data from discrete water jet experiments with those obtained in the whirling arm is not possible (at least not for the coatings of this work). The mechanism of impact and the associated energy absorption appear to be too different in the two setups. The recommendation is therefore that continuous or discrete water jets can be used for a fast initial and crude screening of ideas for new formulations (e.g. a new pigment, binder or filler material), but for actual rankings of different binders or formulations, close to commercialization of a product, the whirling arm or similar rigs should be used.

Nomenclature

d_h	the gap size of slots in the disk (m)
f_D	disk rotation frequency (Hz=s^{-1})
f_{wh}	wheel rotation frequency (Hz=s^{-1})
F_{max}	the maximum force applied during the tensile test
n	number of tested panels, n=10
s	standard deviation
v_j	water jet velocity (m/s)
$\bar{x}$	average value of 10 samples in table 3.2, various units

Subscripts

D	disk for chopping jets
wh	wheel for holding sample panels

References for chapter 3

[1] S.Z. Zhang, K. Dam-Johansen, S. Nørkjær, P.L. Bernad Jr., S. Kiil, Erosion of wind turbine blade coatings – Design and analysis of jet-based laboratory equipment for performance evaluation, submitted to Prog. Org. Coat. , April 2014.

[2] D. Cripps, The future of blade repair, Reinforced Plastics. 55 (2011) 28-32.

[3] G. Marsh, Meeting the challenge of wind turbine blade repair, Reinforced Plastics. 55 (2011) 32-36.

[4] J.G. McGowan, R.W. Hyers, K.L. Sullivan, J.F. Manwell, S.V. Nair, B. McNiff, B.C. Syrett, A review of materials degradation in utility scale wind turbines, Energy Materials. 2 (2007) 41-46.

[5] M. Grundwürmer, O. Nuyken, M. Meyer, J. Wehr, N. Schupp, Sol–gel derived erosion protection coatings against damage caused by liquid impact, Wear. 263 (2007) 318-329.

[6] M. Lesser, The impact of a compressible liquid, in: M. Rein (Ed.), CISM Courses and Lectures, Springer-Verlag Wien, Vienna; Sachsenplatz 4-6, A-1201 Vienna, Austria, 2002, 39-102.

[7] J. Zahavi, S. Nadiv, G.F. Schmitt Jr., Indirect damage in composite materials due to raindrop impact, Wear. 72 (1981) 305-313.

[8] O. Gohardani, Impact of erosion testing aspects on current and future flight conditions, Prog. Aerospace Sci. 47 (2011) 280-303.

[9] J.H. Brunton, M.C. Rochester, Erosion of solid surfaces by the impact of liquid drops, in: C.M. Preece (Ed.), Treatise on materials science and technology, Academic press, New York, 1979, 186-248.

[10] H. Cease, P.F. Derwent, H.T. Diehl, J. Fast, D. Finley, Measurement of mechanical properties of three epoxy adhesives at cryogenic temperatures for CCD construction, Fermi National Accelerator Laboratory. Fermilab-TM-2366-A (2006) 1-19.

[11] Modulus of elasticity - Young's Modulus for some common materials, http://www. engineeringtoolbox. com/young-modulus-d_417. html. (Accessed 15.07.2014).

[12] S. Kiil, Quantification of simultaneous solvent evaporation and chemical curing in thermoset coatings, Journal of Coatings Technology and Research. 7 (2010) 569-586.

Conclusions

The wind power industry has grown fast during the last decade and the future development is expected to bring very large towers and blades to the market. In this thesis, it has been discussed how rain droplets can damage wind turbine blades and it was emphasized that blade coatings can prolong the blade life time by reducing erosion rates.

As with most coating systems, accelerated testing of novel blade coating formulations is an essential requirement. Preferably, testing times should be measured in hours or days as opposed to a service life time of about 20 years. In addition, experimentation costs should not be prohibitive. It has been the aim of the present work to explore the possibilities of designing a novel laboratory setup for blade coating investigations. A discrete water jet principle was chosen and commercial polyurethane-based blade coatings selected for the experiments. Comparison of results with erosion data from the industrial standard, the whirling arm rig, has been part of the research.

The new experimental rig, which uses discrete water jets, is capable of fast screening of up to 22 coating samples simultaneously. A mathematical model was developed to "match" the water hammer pressure and the impact frequency with those of the whirling arm rig. The water jet velocity was found to be the most important parameter for initiation of erosion. Impact frequency, though of less importance, also played a role. However, a simultaneous match of impact velocity and impact frequency did not produce similar coating rankings in the two setups.

Further investigations were conducted on the effects of water cushioning (presence of water film on the coating), substrate curvature, and water nozzle-coating distance. It was found that water cushioning, in some cases, is important and it is recommended to include air blowing (to remove the water film) when using water jet slugs to simulate rain erosion. However, the ranking of coating erosion performance is not a function of water cushioning. Substrate curvature and the water nozzle-coating distance (< 10 cm) did not influence results significantly.

The lack of correlation between the two setups may be attributed to the different erosion modes. The underlying mechanisms of rain erosion are apparently

substantially different in a setup based on impacting water jet slugs and a setup where a rotor arm impacts falling water droplets. Our recommendation is therefore that continuous or discrete water jets can be used for a fast initial and crude screening of ideas for new formulations, but for actual rankings of different binders or formulations, close to commercialization of a product, the whirling arm or similar rigs should be used.

It was found that original defects in the coating and/or the induced small imperfections caused by cumulative fatigue, due to repeated impacts, may act as initiation points and lead to subsequent coating failure during exposure.

Several mechanical measurements to characterize selected blade coatings, including tensile strength, flexibility, impact, hardness, and abrasion experiments, were conducted. Abrasion resistance was found to be an interesting property to correlate with rain erosion data, whereas the other properties investigated did not show any correlation.

Future work

A number of issues are still open and would benefit from further research. These are:

1. A detailed investigation of the whirling arm rig with an emphasis on correlation between laboratory and natural exposure (i.e. full-scale wind turbines). An assumption of this work is that such a correlation exists, but this has not been explored. The investigation is very time-consuming, but over time, data from natural exposure should start to appear, hopefully also in the open literature.

2. Effects of substrate material on rain erosion of blade coatings would be useful to explore. In this work, steel substrates only, which are actually not the most realistic substrate, have been used. Other composite materials should be investigated.

3. High speed camera can be used to record the erosion process, characterize the water jet size and impact velocity. However, the high level humidity in the chamber will be an issue.

4. Other contacting modes could be investigated in the search for a correlation. Scaling down the whirling arm to laboratory-size equipment is probably not realistic due to issues of turbulence and the required amount of droplet generation.

5. Microscopic photos can be taken on whirling arm samples to compare the erosion failure with the one in water jet rig.

Appendix A Detailed instructions for using the water jet erosion equipment

This water jet based erosion equipment was designed and constructed in the Department of Chemical and Biochemical Engineering, the Technical University of Denmark. Depending on the nozzle size, the rig can create water discrete and continuous jets with speed up to 200 m/s, and 22 panels can be tested simultaneously.
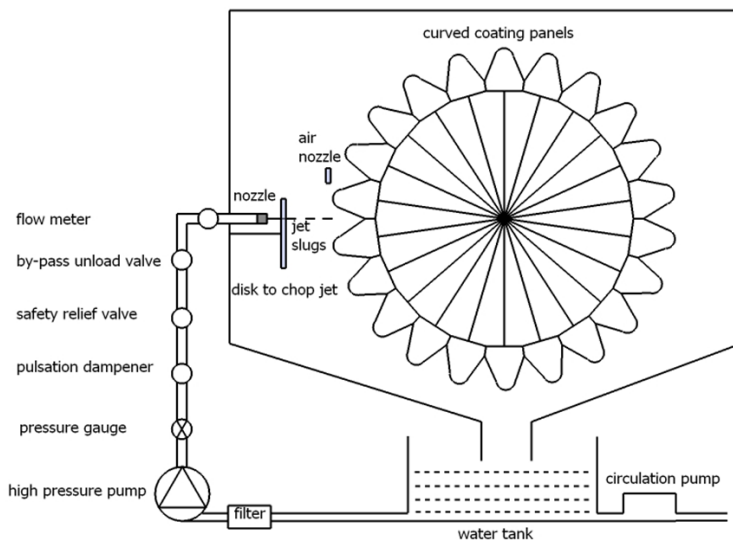

Figure 1 Schematic illustration (vertical cross-sectional view) of water jet erosion rig, including the disk, which ensures discrete water jets. The water recirculation tank holds about 50 liters of water.

To operate the equipment, the following steps should be followed:
1. Check the filter.
2. Connect the electricity supply.
3. Choose the right nozzle and disk; Open the lid of the erosion chamber, screw them in place.
4. Screw the sample panels in the wheel (panel dimension 70×150 mm), switch on the wheel rotation in the control box to rotate the wheel if more panels have to be fixed, close the lid.
5. Connect the water tank with tap water supply and fill the tank with 50 L water.
6. Switch on water pump circulation to keep the water temperature at about 25 ℃.
7. Switch on the wheel and disk rotation at your wanted speeds, and turn on the air supply for the air nozzle and adjust it to your wanted pressure.

A

8. Switch on the high pressure pump, the pressure will be shown on the pressure gauge, regulate the by-pass unload valve to adjust the pressure to your expectation. A stop watch should be started at the same time to record the elapsed time.
9. To stop the experiment, switch off the water pump first, and then turn off the air pressure, wheel and disk rotation. Switch off the circulation pump.
10. Open the lid to observe the panels, or take off the panels.
11. Disconnect the electricity supply and drain off the water in tank.